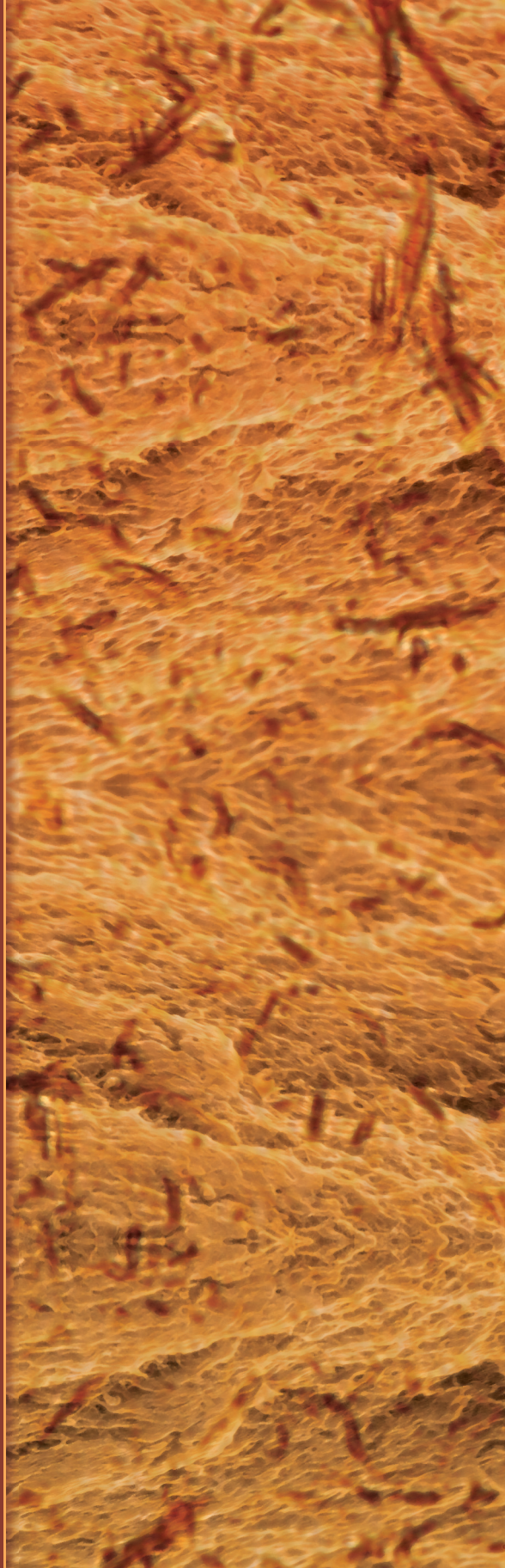


Recent Advances in Polymer Nano- composites

Edited by

S. Thomas
G.E. Zaikov
S.V. Valsaraj

///VSP///



Recent Advances in Polymer Nanocomposites

This page intentionally left blank

Recent Advances in Polymer Nanocomposites

Edited by

S. Thomas, G.E. Zaikov and S.V. Valsaraj

///VSP///

LEIDEN • BOSTON

2009

CRC Press
Taylor & Francis Group
6000 Broken Sound Parkway NW, Suite 300
Boca Raton, FL 33487-2742

© 2009 by Koninklijke Brill NV Leiden The Netherlands
CRC Press is an imprint of Taylor & Francis Group, an Informa business

No claim to original U.S. Government works
Version Date: 20131022

International Standard Book Number-13: 978-1-4665-6372-8 (eBook - PDF)

This book contains information obtained from authentic and highly regarded sources. Reasonable efforts have been made to publish reliable data and information, but the author and publisher cannot assume responsibility for the validity of all materials or the consequences of their use. The authors and publishers have attempted to trace the copyright holders of all material reproduced in this publication and apologize to copyright holders if permission to publish in this form has not been obtained. If any copyright material has not been acknowledged please write and let us know so we may rectify in any future reprint.

Except as permitted under U.S. Copyright Law, no part of this book may be reprinted, reproduced, transmitted, or utilized in any form by any electronic, mechanical, or other means, now known or hereafter invented, including photocopying, microfilming, and recording, or in any information storage or retrieval system, without written permission from the publishers.

For permission to photocopy or use material electronically from this work, please access www.copyright.com (<http://www.copyright.com/>) or contact the Copyright Clearance Center, Inc. (CCC), 222 Rosewood Drive, Danvers, MA 01923, 978-750-8400. CCC is a not-for-profit organization that provides licenses and registration for a variety of users. For organizations that have been granted a photocopy license by the CCC, a separate system of payment has been arranged.

Trademark Notice: Product or corporate names may be trademarks or registered trademarks, and are used only for identification and explanation without intent to infringe.

Visit the Taylor & Francis Web site at
<http://www.taylorandfrancis.com>

and the CRC Press Web site at
<http://www.crcpress.com>

Contents

Preface	vii
1 Preparation, Structure–Property Relationship, and Applications of Layered Silicate Rubber Latex Nanocomposites Siby Varghese and Sabu Thomas	1
2 Polymer–Graphite Nanocomposites Sie Chin Tjong	19
3 Polyaniline Nanocomposites Hartmut Fischer and Jos Kunen	47
4 Polyolefin Clay Nanocomposites Tomas Peprnicek, Lucie Kovarova, and Dagmar Merinska	119
5 PMMA-, PAN-, and Acrylic-Based Polymer Nanocomposites Haitao Wang and Wei Zhong	155
6 Polyurethane Nanocomposites Fabrice Leroux and Anne-Lise Troutier	181
7 Semiconductor–Polymer Nanocomposites V. Djoković, T. Radhakrishnan, P. Sreekumari Nair, M.I. Čomor, and J.M. Nedeljković	227
8 Cellulose Fibril- and Whisker-Reinforced Polymer Nanocomposites Wolfgang Gindl	269
9 Enhancement of Thermal, Thermomechanical, and Mechanical Properties of Carbon-Fiber-Reinforced and Sandwich Composites Through Nanophased Epoxy/Foam Mahesh V. Hosur	285
10 The Cure Behavior of Thermosetting Resin-Based Nanocomposites Characterized by Using Dynamic Torsional Vibration Method Yiyun Cheng, Dazhu Chen, Tongwen Xu, and Pingsheng He	337
11 NMR Investigations on Polymer Nanocomposites J.C.E.M. Grandjean	363

12	Structure Determination of Polymer Nanocomposites by Small-Angle Scattering	
	Julian Oberdisse, Wim Pyckhout-Hintzen, and Ekkehard Straube	397
13	Fire-Retardant Properties of Polymer Nanocomposites	
	Robert A. Shanks and Antonietta Genovese	439
14	Nanocomposite Polymer Electrolytes for Lithium Batteries	
	Arul Manuel Stephan	455
15	Application of Nanocomposites in Imaging and Display Media	
	Debasis Majumdar, Thomas Blanton, and Narasimharao Dontula	483

Preface

There has been enormous interest in the commercialization of nanocomposites for a variety of applications, and several of these will be successful in the near future. Over the last ten years, several different types of polymer nanocomposites have become the dominant class of multicomponent polymer systems. A large number of scientific publications, industrial patents, international conferences, and exhibitions are devoted to this class of materials.

This book mainly focuses on the preparation, properties, characterization, and applications of polymer nanocomposites. The various manufacturing techniques, analysis of morphology, filler dispersion, interfacial interactions, etc. have been described in detail. For nanocomposites, filler dispersion, intercalation/exfoliation, orientation and filler–matrix interaction are the main parameters that determine the physical, thermal, transport, mechanical, and rheological properties of the nanocomposites. The ultimate properties of the nanocomposites have been correlated with the key parameters of filler dispersion and filler–matrix interaction. The use of various sophisticated instrumental techniques for the characterization of these nanocomposites has been reviewed in this book.

Although there are published data and books on polymer nanocomposites, there is no specific book dedicated to all types of nanofillers. It is important to add that none of the existing books cover all range of nanofillers from spherical to two dimensional (0D to 2D fillers). The main objective of this book is to summarize in a fairly comprehensive manner many of the recent technical accomplishments in the area of polymer nanocomposites. The book is intended to serve as a one-stop reference resource for important research accomplishments in the area of polymer nanocomposites. Prominent researchers from industry, academia and government/private research laboratories across the globe have contributed the various chapters in the book. The book will be a very valuable reference source for university and college faculties, professionals, post-doctoral research fellows, senior graduate students, polymer technologists, and researchers from R&D laboratories working in the area of polymer nanocomposites.

Chapter 1 discusses the role of interface, preparation, structure–property relationship, and applications of layered silicate rubber latex nanocomposites. The interface has a strong influence on the properties of polymer nanocomposites. The influence of various compatibilising agents and interfacial agents on the morphology, structure and properties has been discussed in detail. The polymer–filler interaction and filler dispersion on the properties of the nanocomposites have been correlated with the interface.

The structure, mechanical, electrical, and thermal characteristics of polymer–graphite nanocomposites has been discussed in Chapter 2. The graphite structure and property modification by methods like intercalation with alkali metals followed by exfoliation with aqueous solvents, inserting sulfuric acid between the carbon layers of graphite to expanded graphite, heat exfoliation of the graphite, and ultrasonication to separate loosely connected graphite nanosheets into individual nanoplatelets are discussed. The mechanical

and electrical properties of graphite polyamide nanocomposites, graphite polypropylene nanocomposites, and graphite epoxy nanocomposites are discussed in the chapter. Chapter 3 mainly concentrates on three types of PANi-containing nanocomposites: (1) composites with nanostructured materials, such as clay and certain metal compounds of which the cavities have been filled with PANi by *in situ* polymerization or impregnation techniques, (2) composites with nanoscaled metal particles, metals oxides and silica particles embedded in PANi, (3) composites with carbon nanotubes and graphite. Their properties and applications are also elaborated in this chapter.

Chapter 4 briefly describes the theoretical reason of modification of either nanoclays or polymeric matrix for the preparation of high performance nanocomposites. The chapter deals with polypropylene, polyethylene, and EVA copolymer nanocomposites. The various processing conditions which affect morphology and final characteristics of prepared nanocomposites has been elaborated. The morphological, mechanical, and thermal characterization of the above-mentioned polymer nanocomposites are also discussed in the chapter. Chapter 5 emphasizes the preparation and characterization of PMMA, PAN and the other acrylic-based polymer nanocomposites by the addition of inorganic nanofillers. The mechanistic understanding of the different preparation approaches and the effects after the addition of various inorganic nanoparticles and their potential applications are elaborated here.

Chapter 6 reports the state of the art regarding polyurethane (PU) nanocomposites, from processing and characterization to specific properties and end-use applications. The different parameters determining PU nanocomposites are studied in detail. In this chapter, nanocomposites based on thermoplastic or waterborne PU, PU foams, blends of polymers, and fillers both “inert” or “reactive” have been elaborated. The correlation between the fundamental nanocomposite structure and properties such as mechanical, permeation, barrier, thermal stability, flame retardancy etc. have been established by taking into consideration the filler–volume fraction as well as the aspect ratio. The emerging applications of PU nanocomposites in the biomedical field and other contemporary domains are also presented in this chapter.

Chapter 7 covers major activities for designing novel nanoarchitectures for emerging technologies with emphasis on synthesis, structure and optical properties of polymer–metal chalcogenide (CdS, PbS, CdSe, HgS, and Ag₂S etc.) nanocomposites. Basic synthetic routes and typical polymer matrices (homopolymers, random- and block-copolymers, conductive polymers, and biopolymers) are considered. The role of the surface fictionalizations of semiconductor nanoparticles as a means of preparing ordered composite structures is also discussed. Concerns of possible influences of semiconductor nanoparticles on the physical properties of the host matrix are also addressed.

It has been demonstrated that the addition of a small quantity of cellulose whiskers to various polymers greatly improves their dynamic mechanical properties in particular their stiffness at $T > T_g$ of the matrix. At higher fiber content, composites with impressive mechanical properties (modulus up to > 25 GPa, strength > 450 GPa) were obtained using nanofibrillated wood pulp and bacterial cellulose. In Chapter 8, a brief review of the literature on the production, structure, and properties of cellulose whiskers and nanofibrils together with their polymer composites is given.

Rapid progress made in the synthesis and development of nanoscale materials has motivated researchers to alter the constituent phases of traditional fiber-reinforced composites and sandwich constructions with the nanosized fillers. In Chapter 9, recent developments made in the field of polymeric nanocomposites for structural material applications

are reviewed. This article reveals the recent progress made in the field of nanotechnology as applied to structural polymeric composites. Particular focus is given to carbon-fiber-reinforced nanophased composites and sandwich constructions. The article elaborates the modification of matrices, modification or the synthesis of nanophased fibers, the modification of foam and the fabrication of nanophased structural-fiber-reinforced and sandwich composites. Emphasis is given to the evaluation of thermal, thermomechanical, mechanical (both quasi-static), and dynamic properties.

A better understanding of the chemorheology of the unfilled or filled thermosetting resins is of great importance to many industries including integrated chip manufacturers, aerospace technologies, automotive manufacturers, and many other specialized applications. Convenient and rapid techniques for the determination of chemorheology and cure kinetics can lead to a better understanding of the cure processing of thermosetting-resin-based nanocomposites. This will provide enough experimental data to optimize these processes and thereby reduce design and operating costs in the industry. Mechanical methods such as the dynamic torsional vibration method (DTVM) can be used successfully to investigate the curing process in several thermosetting resin systems. Chapter 10 highlights the utilization of DTVM to study the cure behavior of several thermosetting-resin-based nanocomposites, with particular reference to layered silicate-reinforced polymer nanocomposites.

NMR can be used in different ways to investigate composites of polymers with inorganic compounds and diverse polymer nanocomposites. Nanocomposites may contain noncrystalline and crystalline phases. NMR allows the determination of their relative contents and description of their different motional properties. NMR can also discriminate between the different crystalline forms in these systems. Chapter 11 gives a brief survey of NMR theory required to investigate polymer nanocomposites. It also describes the NMR studies of solid polymer electrolytes, nanocomposites prepared with conducting polymers, and the characterization and dynamics of the nanocomposites or some of their precursors.

The characterization of the structure of polymer nanocomposites by the techniques of small-angle scattering of neutrons and X-rays is reviewed in Chapter 12. This review focuses on structure determination in polymer nanocomposites by scattering methods, namely small angle neutron scattering and small angle X-ray scattering. It concentrates on the case of soft and continuous polymer matrices with inclusions of hard, nanometric filler particles like carbon black, silica and silicates.

Nanocomposites have been shown to contribute to certain flame retardant mechanisms where their high surface area to volume ratio gives an advantage, and some unique fire retardant attributes are added. Chapter 13 considers the mechanism of degradation and combustion, and then provides examples of the type of additives that can retard the combustion process at each stage. Synergisms between additives are included and explained. Recent examples of nanocomposites and hybrids of nano- and micro-composites are provided where the nanoparticles enhanced fire retardance.

The rapid growth of the miniature electronic and computer-related industries has caused great demand for smaller and lighter batteries with high level of energy and safety characteristics. Chapter 14 reviews the state-of-the-art of nanocomposite polymer electrolytes and encompasses their electrochemical and physical properties for the applications in lithium-polymer batteries especially for elevated temperature applications. The experimental procedure and the role of nanofillers on the ionic conductivity, compatibility with lithium metal anode and their cycling ability are discussed in this chapter. The electrochemical characteristics such as electrochemical impedance, transference number,

interfacial properties of Li/CPE/Li cells, and the cycling behavior of PVdF–HFP nanocomposite electrolytes with transition metal oxide cathode materials are also discussed.

The unique physical properties of nanocomposites have been explored by several industrial sectors. Chapter 15 looks at clay–polymer-based nanocomposite materials for applications in multilayered imaging elements and display components. The chapter mainly focuses on clay–polymer-based nanocomposite materials for applications in multilayered imaging elements and display components. The applications of clay–polymer nanocomposites in photographic and inkjet media and display components are well illustrated.

1 Preparation, Structure–Property Relationship, and Applications of Layered Silicate Rubber Latex Nanocomposites

Siby Varghese and Sabu Thomas*

Rubber Technology Division, Rubber Research Institute of India, Kottayam, Kerala, India; School of Chemical Sciences, Mahatma Gandhi University, Kottayam, Kerala, India

1.1 Introduction

Polymeric nanocomposites can be considered as an important category of organic–inorganic hybrid materials, in which inorganic nanoscale building blocks (e.g., nanoparticles, nanotubes, or nanometer-thick sheets) are dispersed in an organic polymer matrix [1–5]. When compared to conventional composites based on micrometer-sized fillers, the interface between the filler particles and the matrix in polymer nanocomposites constitutes a much greater area within the bulk material, and hence influences the composite's properties to a much greater extent, even at a rather low filler loading [6–8]. Polymer nanocomposites reinforced by relatively small amounts of ultrafine nanoparticles (most often clay platelets) proved exceptionally promising engineering materials with unexpectedly high stiffness–toughness ratio, gas barrier properties, flame retardance, etc. The real interest in nanotechnology is to create revolutionary properties and functions by tailoring materials and designing devices on the nanometer scale.

According to a report, the total worldwide market for polymer nanocomposites reached 11.1 million kg worth 90.8 million US\$ in 2003. This market is expected to expand at an average annual growth rate of 18.4% to reach 211 million US\$ by 2008.

* Correspondence should be addressed to e-mail: sibyvarghese100@yahoo.com

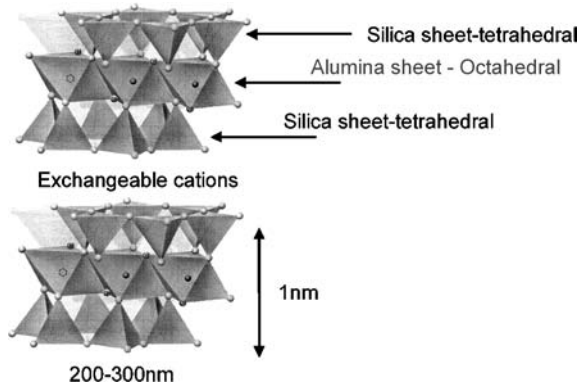


Figure 1.1. Schematic representation of (tetrahedral–octahedral–tetrahedral) montmorillonite (MMT) clay [3].

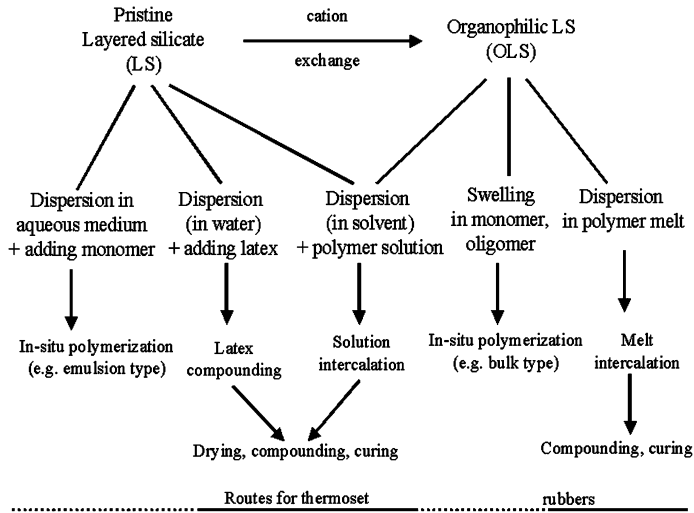
Polymer-layered silicate nanocomposites (PLSN) are the foremost members of such high-performance nanocomposites. Improvements in mechanical, thermal, and barrier properties, flame retardancy, etc., are claimed for this class of polymer nanocomposites that could not be achieved by conventional fillers at such low loading (typically <10 phr). This class of material uses different types of clay, such as smectite, laponite, kaolinite, etc., among which smectite group of clays are most widely used due to its layered structure, very high surface area (700–800 m²/g), higher cation exchange capacity (90–125 meq/100 g clay), and high aspect ratio (100–300). Cations like ammonium ion with long aliphatic hydrocarbon chains compatibilize the silicates with polymers and enhance the interaction with a polymer by enlarging the interlayers (lamina), generating organically modified layered silicates (LS) or simply organoclays. Each layer is constructed from a two-silicon tetrahedron fused to an alumina octahedron (Figure 1.1).

1.2 Production of Rubber–Clay Nanocomposites

Currently, numerous procedures for the preparation of polymer nanocomposites have been proposed [3–8], using the following approaches:

- Direct intercalation of nanoscale building blocks into a polymer melt or solution.
- *In situ* generation of nanoscale building blocks in a polymer matrix.
- Polymerization of monomers in presence of nanoscale building blocks.
- A combination of polymerization and formation of nanoscale building blocks (e.g., sol–gel method, intercalation of monomers into layered structures followed by polymerization, etc.).

The key issue of these techniques is that the geometry, spatial distribution, and volume content of the nanofillers must be effectively controlled through adjusting the preparation conditions to ensure the structural requirements of nanocomposites. The preparation of rubber–clay nanocomposites slightly differs from the above scenario as some methods are not ideal (e.g., *in situ* polymerization) and rubbers are available in various forms (latex, solution, and dry), which offer additional possibilities (e.g., latex compounding). Scheme 1.1 shows the possible production routes of thermoset–rubber–LS nanocomposites. Further, the melt intercalation method, which is strongly recommended for dry form



Scheme 1.1. Possible preparation routes of rubber-layered silicate nanocomposites [4].

of rubber, is not included here as the main theme of our discussion is latex-based nanocomposites [4].

Modification of the clay by organic molecules (“organophilization”) is not always a necessary step in the production of polymer nanocomposites. In general, two types of organic–inorganic hybrids are distinguished – intercalated (in which polymer chains are diffused between the silicate layers) and exfoliated (in which the silicate layers of ca. 1 nm thickness are fully delaminated and dispersed in the polymer matrix). Pristine-layered silicates usually contain hydrated Na^+ or K^+ ions. In aqueous dispersions, the clay “swells” (i.e., its layers are separated due to hydration of the interstitial cations), which facilitates the intercalation of the rubber molecules when the dispersion is mixed with latex.

It is further emphasized that a dramatic improvement in the properties of polymer–clay nanocomposites can only be achieved by ensuring the initial penetration (intercalation) of polymer molecules into the interlayer space (galleries) of clay tactoids and subsequently by forcing these layers apart to complete delamination (exfoliation) of the clay monolayers (1 nm thickness) throughout a polymer matrix. Apparently, the major outcome of this technology is the achievement of a maximum possible area for polymer–filler interaction by eliminating the initial aggregated state of clay nanolayers.

1.3 Characterization of Nanocomposites

1.3.1 X-Ray Diffraction Technique

X-Ray diffraction (XRD) is the most widely used technique for the characterization of polymer nanocomposites [7,8]. The change in the interlayer spacing, that is, “ d ” spacing of the latex nanocomposites, is observed from the peak position in the XRD pattern in accordance with the Bragg’s equation

$$n\lambda = 2d \sin \theta, \quad (1.1)$$

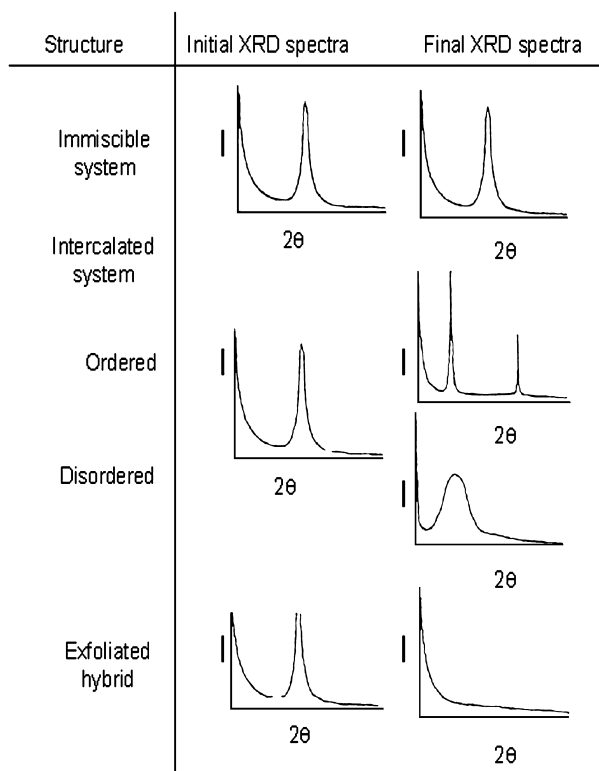


Figure 1.2. Schematic representation of XRD spectra of possible polymer-layered silicate nanocomposites structures [7,8].

where n is the order of diffraction, λ is the wavelength of X-rays, d is the interlayer spacing, and θ is the angle of diffraction. The XRD method has been used to characterize the formation of structure in polymer–silicate hybrids by monitoring the position, shape, and intensity of the basal reflection from the silicate layers. Figure 1.2 summarizes the general character of the X-ray spectra for various types of PLSN structures. For immiscible mixtures of polymer and organophilic-layered silicates (OLS), the basal reflection does not change upon blending with the polymer. On the other hand, the finite-layer expansion associated with intercalated structures results in a new basal reflection that corresponds to the larger gallery height. A decrease in the degree of coherent layer stacking (i.e., a more disordered system) results in peak broadening and intensity loss. In contrast, the extensive layer separation, beyond the resolution of Bragg–Brento geometry, of exfoliated structures does not result in a new, observable, basal reflection [7,8].

1.3.2 Transmission Electron Microscopy

Transmission electron microscopy (TEM) is a powerful technique used for the characterization of PLNC. It gives a direct measure of the spatial distribution of silicate layers, morphology, and structural effects of a selected area of the sample; however, the limitation is that it requires substantial skill in specimen preparation and analysis. Figure 1.3 shows

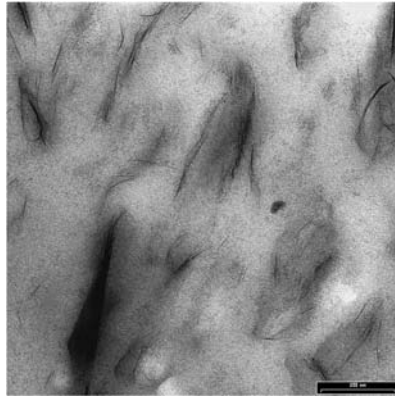


Figure 1.3. TEM picture of natural rubber (NR) nanocomposites containing 10 phr MMT-ODA (note that ODA is octadecyl amine used as modifier for MMT) [9].

the exfoliation of LS (MMT-ODA) at a loading of 10 phr [9]. Here, the black strands-like portion in the photograph shows the fully separated silicate sheets.

1.3.3 Differential Scanning Calorimeter

Differential scanning calorimeter (DSC) measurements of PLSN are helpful for the identification of the extent of intercalation. The interactions of the intercalated polymer chains with the host species reduce its segmental mobility, thereby increasing its glass transition temperature T_g up to five units. Accordingly, PMMA/organically modified MMT shows increase in T_g with MMT content [10]. It is due to the confinement of the intercalated polymer chains between the sheets of the clay that prevents the segmental motions of the polymer chains’.

1.3.4 Dynamic Mechanical Thermal Analysis

Similar to DSC, dynamic mechanical thermal analysis (DMTA) can also provide information about the T_g of PLSN. The magnitude of the storage modulus (E') gives an idea about the level of reinforcement, and hence the intercalation in MMT-ODA and MMT-TMDA composites compared to the microcomposite – NR–silica system (Figure 1.4). It is also reported that damping peak in the $\tan \delta$ curves decreases upon the addition of silicates due to the restricted mobility of chain segments (Figure 1.5). Moreover, dynamic mechanical studies on MMT-ODA systems indicate the presence of a separate relaxation event, which has been attributed to less-mobile chains within the interfacial region [9]. This may be due to the higher level of intercalation in MMT-ODA (interlayer distance 2.10 nm) compared to MMT-TMDA (interlayer distance 1.85 nm).

1.3.5 Transport Properties

Due to the large aspect ratio of the LS, the permeability of PLSN decreases drastically. The substantial decrease can be explained by the increase in tortuosity of the path of the gas as it diffuses into the nanocomposite [11]. The barrier improvement is predicted by tortuous path model to be a function of the volume fraction ϕ and the aspect ratio of the

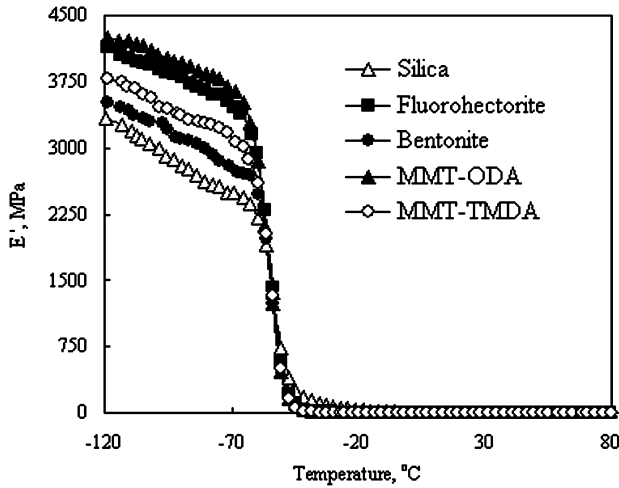


Figure 1.4. Complex storage modulus (E') as a function of temperature for different silicate-filled NR nanocomposites [9]. Note that ODA is octadecylamine and TMDA is methyl tallow bis-2-hydroxyl ethyl quaternary ammonium, used as modifiers for MMT.

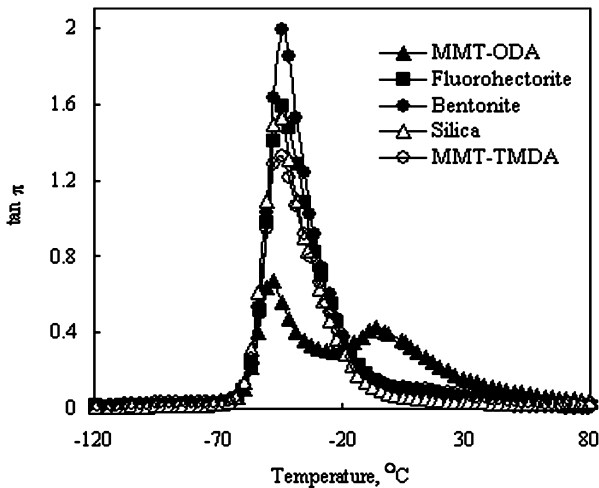


Figure 1.5. Mechanical loss ($\tan \delta$) as a function of temperature for different silicate-filled nanocomposites [9]. Note that ODA is octadecylamine and TMDA is methyl tallow bis-2-hydroxyl ethyl quaternary ammonium, used as modifiers for MMT.

silicate layers α ; higher aspect ratios provide greater barrier improvements according to the following equation for permeability:

$$PN = \frac{(1 - \phi) \times PM}{1 + \alpha\phi/2}, \quad (1.2)$$

where PN represents the permeability of the resulting nanocomposites and PM the permeability of the matrix polymer. Toyota researchers reported that the water absorption of

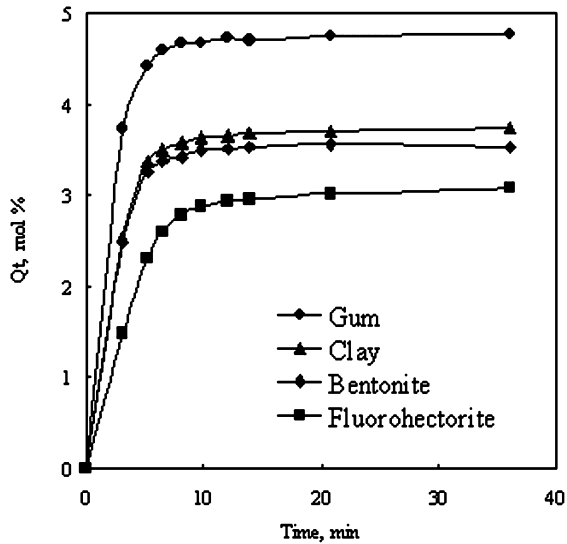


Figure 1.6. Swelling behavior of the LS-filled (nano) composites in toluene at 25 °C [18].

nylon–clay hybrid reduced by 40% as compared to the pure polymer [12]. The gas permeability in rubber–clay hybrids was also reduced by 30% with 4 vol.% of exfoliated clay [13]. There is substantial reduction in free volume upon the addition of nanofillers to polymer matrix due to the increased polymer–filler interaction [14]. The dispersed nanocomposites exhibit increased solvent resistance compared to immiscible hybrids (Figure 1.6). The exfoliated silicate layers prevent solvent molecules to diffuse and damage the polymer network [15].

1.3.6 Thermal Stability

The thermal stability of nanocomposites increased with the amount of silicate layers in the composites [16]. Polymer–clay nanocomposites were characterized by a single weight loss with the beginning of the degradation shifted to much higher temperature. A possible reason for the high thermal stability of nanocomposites might be the well-dispersed inorganic material (silicate) with high thermal stability and great barrier properties, which prevent the heat to transmit quickly and limit the continuous decomposition of the nanocomposites.

1.3.7 Fourier Transmission Infrared Spectroscopy

Fourier transmission infrared spectroscopy (FT-IR) can be effectively used for the characterization of PLSN. This is essentially due to the shift in the Si–O stretching (1005/cm) and Si–O bending (476/cm) vibrations (frequency) to lower wavelengths [17] (Figure 1.7) due to the interaction of the silicate (intercalation/exfoliation) with the polymer in the composite.

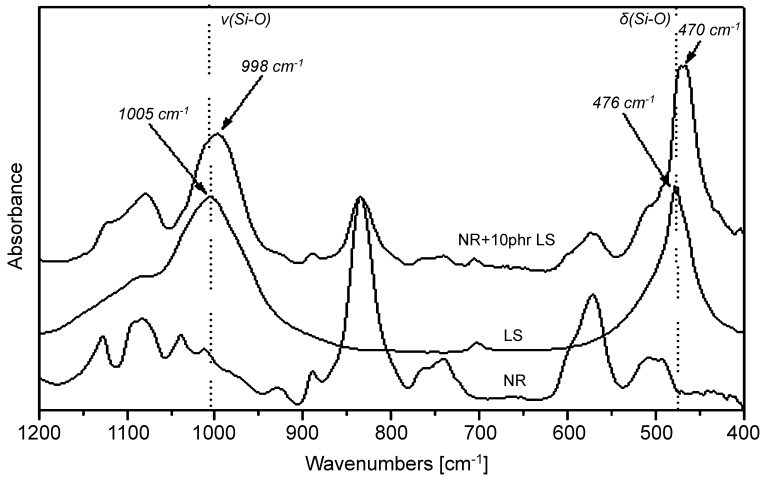


Figure 1.7. FT-IR spectra of fluorohectorite and NR nanocomposite at 10 phr silicate loading [17].

1.4 Properties of Polymer-Layered Silicate Nanocomposites

The great importance in the field of PLSN arises due to the dramatic improvement in mechanical and physical properties of polymer nanocomposites. The improvement in properties widely reported for nanocomposites include increased modulus, reduced gas permeability, greater resistance to solvents, and elevated ion conductivity. The improvement in mechanical properties such as tensile strength, tensile modulus, and young modulus of PLSN can be related to the degree of exfoliation of the LS in the polymer matrix. The enhancement in mechanical properties provided by exfoliated nanocomposite structure on polyamide 6 (PA 6) clay hybrids was first reported by the Toyota researchers [12]. The modulus was increased by 90% and tensile strength by 55% with the addition of 4 wt.% of exfoliated clay.

1.5 Natural Rubber Latex Nanocomposites

As most of the rubbers exist in latex form and LS can be easily dispersed in water, the production of nanocomposites from latices was rather easy. Here the latex should be blended with the clay–water slurry without causing coagulation of the rubber. Production of nanocomposites from NR latex by compounding method has been reported [17, 18]. Two types of LS, namely sodium fluorohectorite (LS of synthetic origin having high aspect ratio) and sodium bentonite (LS of natural origin), are ideal for latex incorporation. Suitably dispersed organoclays (modified silicates) are also good for latex compounding. Dispersions of the LS were prepared and compounded with NR latex along with dispersions of other rubber chemicals for vulcanization. An inert-filler-loaded (nonlayered clay) NR latex composite was used as reference material.

LS showed excellent dispersion in NR latex as compared to conventional composites. The dispersion of LS in the nanocomposites was observed by TEM and was illustrated in Figures 1.8a and b. The related TEM pictures represent the nonlayered clay (Figure 1.8a) and sodium fluorohectorite-filled NR (Figure 1.8b) composites, respectively. In the non-

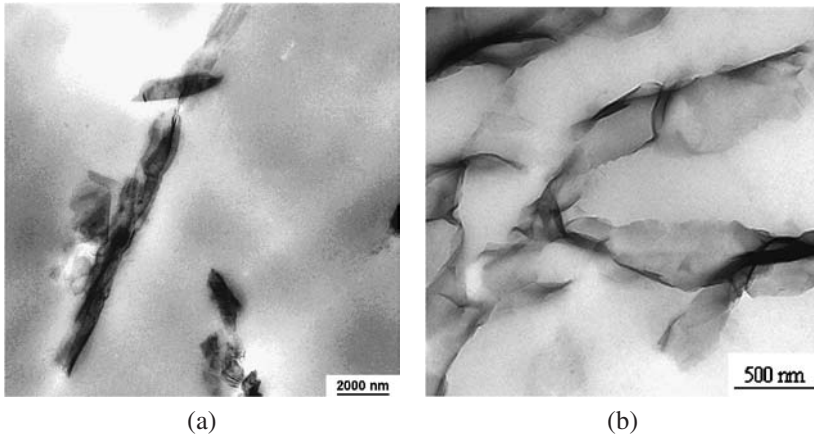


Figure 1.8. TEM photographs of nonlayered (a) and LS (b) prepared from sulfur-vulcanized NR latex nanocomposites at a loading of 10 phr fluorohectorite [18].

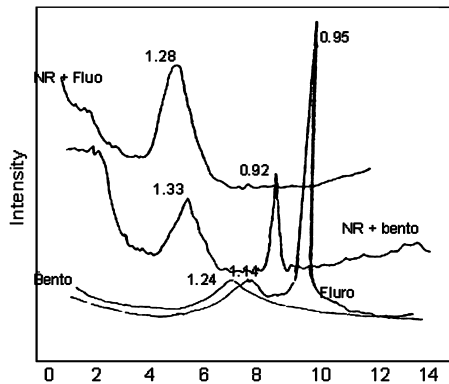


Figure 1.9. XRD pattern of pristine-layered silicates (fluorohectorite and bentonite) and that of the corresponding NR nanocomposites at 10 phr loading.

LS-filled composites, the filler was dispersed as large agglomerated particles (Figure 1.8a), whereas fluorohectorite exists as thin silicate sheets (Figure 1.8b).

Even though the layers are “inorganic” in nature, because of their very large aspect ratio and nanometer thickness, they behave mechanically more like thin sheets rather than thick rigid plates. This flexibility (elastic nature) of the silicate layers contributes to the elasticity of the rubber. It has been reported that intercalated and exfoliated clay layers in rubber orient along the strain direction during stretching.

The XRD spectrum of pure clay and that of the NR latex nanocomposites (10 phr loading) is given in Figure 1.9. Sodium bentonite exhibits a single peak at 7° , which corresponds to a basal spacing of 1.24 nm. Sodium fluorohectorite has two peaks, one at 8° and the other at 9.5° corresponding to a basal spacing of 1.14 and 0.95 nm, respectively. As shown in Figure 1.9, the basal spacing of Na-bentonite-filled NR is shifted to 1.33 nm, indicating that the NR chains get intercalated into the galleries of Na-bentonite. The peak at 0.92 might result from the unintercalated clay layers. Fluorohectorite-filled NR shows a

broad peak at a basal spacing of 1.28 nm. Enhanced interlayer distance indicated that the layered structure was retained because of the formation of intercalated nanocomposite.

The enhancement in moduli at various elongations of NR latex nanocomposites produced by compounding method was given in Figure 1.10. Two types of LS and one nonlayered version were used for the study. Depending upon the nature of the clays, there was increase in the moduli at various elongations for all the composites. However, significant increase in moduli was noted for fluorohectorite-loaded nanocomposites.

The dynamic mechanical properties of PLSN depend mainly on the extent of intercalation and exfoliation. On the other hand, a remarkable increase in the storage modulus was noticed for both LS-filled composites compared to the nonlayered version (Figure 1.11). Substantial increase was noted in the storage modulus of rubber-layered silicate nanocomposites. It was found that the transport of gases through LS-filled latex membranes was lower than conventional microcomposites.

The barrier enhancement can be seen in the case of LS-filled systems than the micro-filled system (Figure 1.12). Upon the addition of 5 phr of fluorohectorite, there was 80%

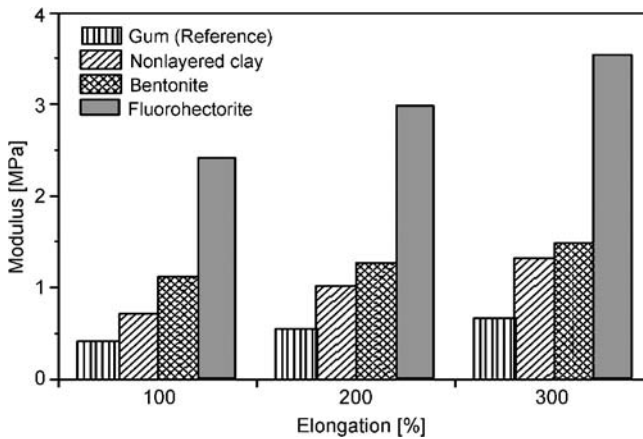


Figure 1.10. Moduli at various elongations of nonlayered and layered silicate nanocomposites [4].

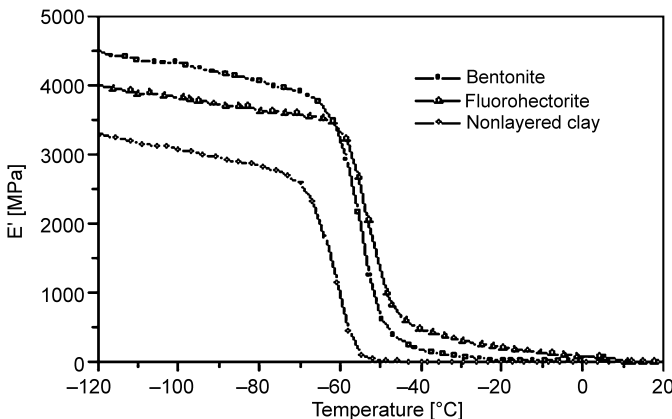


Figure 1.11. Storage modulus at various elongations of nonlayered and layered silicate nanocomposites.

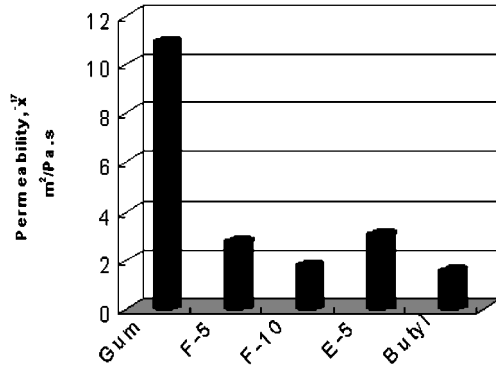


Figure 1.12. Air permeability of various layered and nonlayered silicate NR nanocomposites.

reduction in the permeability compared to the pure NR latex film. This was again reduced when the fluorohectorite content was increased to 10 phr. Almost the same level of reduction was noticed with bentonite-incorporated nanocomposites. This is on par with the air permeability of virgin butyl rubber, which has excellent air impermeability and finds applications in tyre inner tubes. The LS enhance the gas barrier of polymers according to a tortuous path model, in which the LS obstruct the passage of gases and other permeants through polymer matrix [11].

The enhancement in gas barrier properties of layered-clay-reinforced latex membranes indicates strong polymer–filler interaction resulting in more tortuous path for the permeant molecules to travel through the membranes. Since the chain segments get immobilized in the presence of LS, the free volume decreases, thereby reducing the gas permeability coefficient.

1.6 Prevulcanized NR Latex Nanocomposites

The prevulcanized NR latex is an important raw material for the production of many dipped goods. Approximately 600,000 tones of latex concentrate are consumed in this way. Sulfur prevulcanized NR nanocomposite was produced by mixing dispersions of LS with prevulcanized latex. It was found that modulus and tear strength of the vulcanizate increased with incorporation of LS. The threshold loading of LS for enhanced mechanical properties was found to be 3 phr. Higher loading led to agglomeration of filler in the rubber. The solvent resistance of the material was better compared to the nonlayered version.

1.7 Radiation Vulcanized Natural Rubber Latex

Radiation vulcanized natural rubber latex (RVNRL), where the hydrocarbon chains were linked directly through single bonds by γ -radiation, is well noted for its nonallergenic nature. The stress–strain curves of RVNRL composites containing different types of LS are depicted in Figure 1.13. It can be seen that the gum compound (reference) has the lowest stress at all strain levels except at the breaking point where the strain-induced crystallization plays a major role. As the content of sodium fluorohectorite (LS) increases, the stress–strain curves shift toward higher stress values. It is to be noted that the effect of 10-phr-loaded, nonlayered commercial clay was less than 3 phr sodium fluorohectorite.

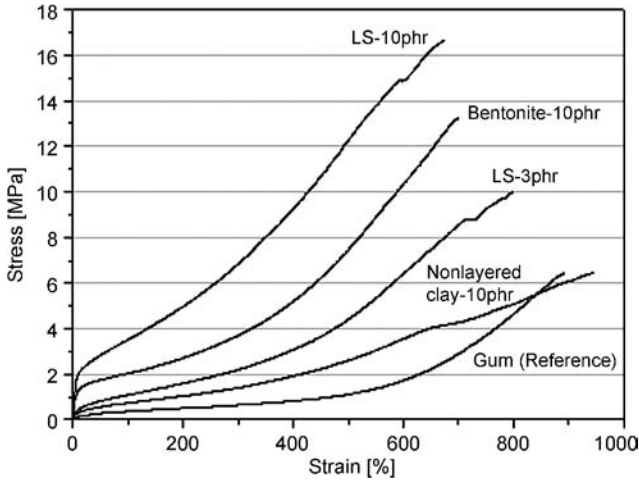


Figure 1.13. Stress–strain curves of nonlayered and layered silicate-filled radiation-vulcanized nanocomposites [4].

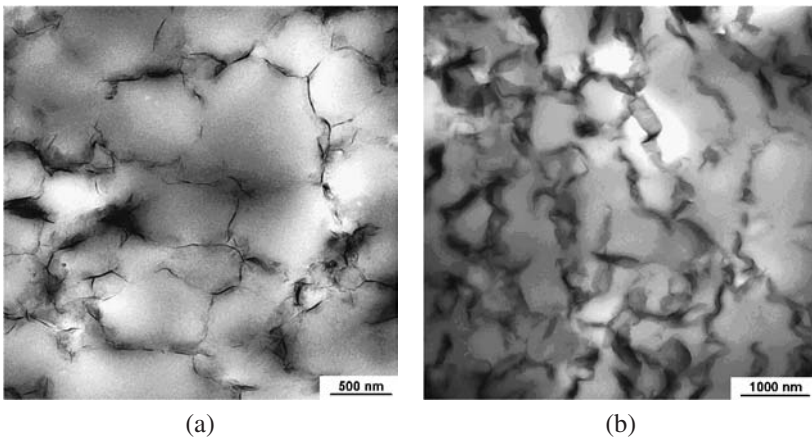


Figure 1.14. TEM photographs of nonlayered and layered silicate nanocomposites based on radiation-vulcanized latex at a loading of 10 phr [4].

The high surface area achieved through exfoliation of LS is the reason for this behavior. The stress at lower elongations (which is a good measure of the reinforcement) is high for all LS-filled nanocomposites, especially for those with sodium fluorohectorite. Note that unlike microcomposites, the ultrathin silicate layers generated by exfoliation of the LS may align along the stress direction without hindering the stress-induced crystallization.

The TEM pictures of the RVNRL nanocomposites loaded with 10 phr each of bentonite and fluorohectorite are given in Figures 1.14a and b. It can be seen that the silicate layers in both the versions are exfoliated well in the latex. This is in agreement with the stress–strain behavior depicted in Figure 1.14. Since the slurry with LS was added to some vulcanized latex, the cross-linked rubber can hardly diffuse into the silicate gallery region. As a consequence, the silicate layers are mostly located in the boundary regions between the NR particles. This ribbon shape offers higher aspect ratio for fluorohectorite

(i.e., larger lateral dimension) compared to bentonite. This, in fact, can be the reason of the outstanding mechanical properties of the related nanocomposites.

1.8 Nanocomposites from Latex Blends

Blending of polymers in the latex stage will give a final product with better properties, depending on the miscibility and properties of individual components. The main advantage of latex stage blending is the finer scale dispersion of the components. The properties of LS-reinforced NR and polyurethane rubber (PUR) latex blends were extensively studied [17].

PUR, being polar and having low molecular mass compared to NR, was supposed to intercalate better with LS. Moreover, addition of PUR latex to NR latex can make the former cheaper without affecting the mechanical properties. Latex blends with various PUR/NR ratios (PUR/NR = 1/1 and 8/2), and with and without LS were produced by film-casting method. Figure 1.15 shows the XRD spectra of the LS and the LS-containing films of various compositions. LS have been intercalated by NR in the related compound as the interlayer distance of the LS increased to 1.19–1.31 nm.

The appearance of the related broad peak suggests that the degree of NR intercalation is different. A considerably better intercalation was noticed for the PUR latex where two peaks were resolved. The major peak indicates that the interlayer distance of the LS widened to 1.73 nm from the initial 0.95 nm. This effect can be assigned to the higher polarity of PUR compared to NR, which favors the compatibility with LS. Similar to PUR, the NR/PUR latex blend showed two XRD peaks at slightly higher interlayer distances.

TEM pictures in Figures 1.16a and b show the good intercalation of LS by PUR. One may get the impression that a part of LS has been even exfoliated. Picture in Figure 1.16b demonstrates further high aspect ratio of the LS used (synthetic sodium fluorohectorite). The dispersion of LS in PUR/NR (1/1) latex blend differs considerably from that of the PUR. TEM pictures in Figure 1.17 shows that NR and PUR are not compatible. The particles from the sulfur-pretreated NR appear dark in these TEM images. LS stacks can be located at the boundary of the PUR (light) and NR (dark) phases. Pronounced intercalation and possible exfoliation took place only in the PUR phase (Figure 1.17b).

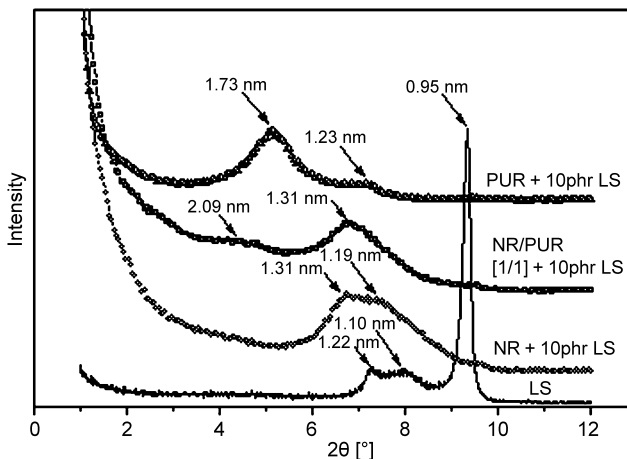


Figure 1.15. XRD spectra of the LS-reinforced latex nanocomposites of various compositions [17].

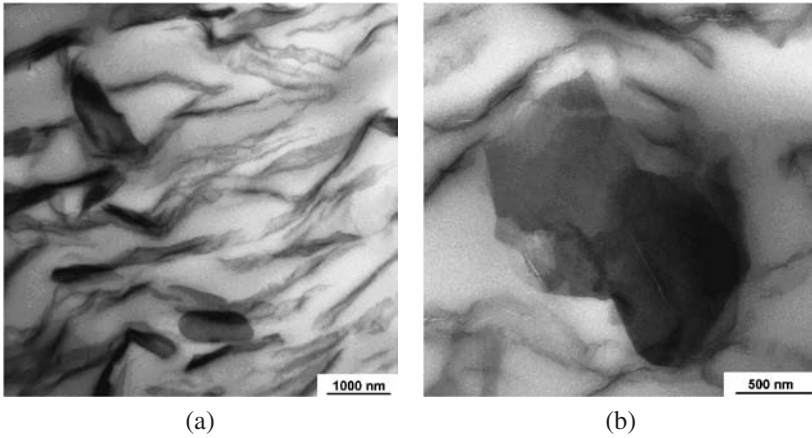


Figure 1.16. TEM images at various magnifications from the cast film of polyurethane latex containing 10 phr LS [17].

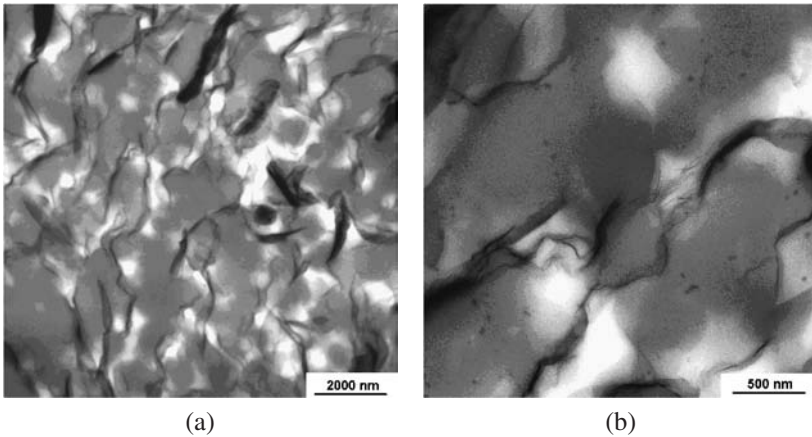


Figure 1.17. TEM images taken from the cast film of PUR/NR (1/1) latex blend containing 10 phr LS [17].

The silicate layers and aggregates cover the NR particles resulting in a skeleton (“house-of-cards”) structure. This results in a skeleton morphology, as the length of the silicate layers is higher than those of the diameter of the particles (Figure 1.17). The formation of this skeleton structure yields improved mechanical properties. A 1:1 blend of PUR and NR latex having 10 phr LS showed three-fold increase in tensile properties compared to virgin polyurethane. Similarly, tear strength of the nanocomposite (1:1 blend) is higher than the corresponding virgin polymer nanocomposites.

1.9 Synthetic Rubber Latex Nanocomposites

PLSN can also be prepared from synthetic latices. Acrylic-latex–nanosilica composites have higher T_g and better tensile properties [19]. These composites showed reduced transmittance of UV radiation. Another method for preparing latex nanocomposites is the coagulation of latex and LS followed by compounding using a two-roll mill. Nanocom-

posites were also made from styrene–butadiene rubber (SBR) and styrene–vinylpyridene latices by coagulation followed by drying. Although the composites showed some level of intercalation, the properties of the resulting nanocomposites were not promising, whereas rectorite–SBR nanocomposites prepared by co-coagulating SBR latex and rectorite water suspension showed excellent gas barrier properties due to the nanometric level dispersion of rectorite [20]. The structure and properties of NR and chloroprene-rubber–clay nanocomposite by coagulating the rubber latex and clay aqueous suspension was also reported [21].

1.10 Solvent-Assisted Intercalation

Melt intercalation of high-molecular-weight polymers is a powerful approach to produce polymers reinforced by organophilic-layered silicates (OLS). This method was quite generally adopted and broadly applicable to a range of commodity polymers. This melt compounding method can be applied to dry forms of rubbers. On the other hand, the dispersion of the silicate can strongly improved by solvent-assisted techniques. In the latter case, the dry rubbers are dissolved in suitable solvents and OLS is added. The OLS swells more or less (depending on the organophilic intercalant used) in the solvent, as well. After solvent removal, the intercalated rubber is compounded with curatives and then vulcanized at specific temperature (Scheme 1.1). This method can thus be referred as a solvent-assisted melt compounding.

Ganter and co-workers prepared rubber nanocomposites based on butadiene rubber (BR) and SBR containing OLS [22]. Here, OLS were swollen in rubber–toluene solution. The increase in interlayer distance of the silicates was monitored by wide-angle X-ray scattering (WAXS). The interlayer distance increased from the initial 1.26 nm (pristine MMT) to 2.59 nm for the organoclay. The interlayer distance ranged from 3.59 nm to approximately 6 nm for the rubber-swollen organoclay. Fully vulcanized nanocomposites were prepared by compounding the rubber-intercalated silicates with chemicals in a two-roll mill followed by vulcanization at 165 °C for 35 min in hot press under vacuum. The excellent dispersion of organoclay (exhibiting intercalated and partially exfoliated layers) in rubber was demonstrated by TEM and atomic force microscopy (AFM).

The research group at Toyota Central Laboratories prepared an organophilic MMT via cation exchange through amine-terminated liquid nitrile rubber (Hycar[®] ATBN) [23]. The exchange reaction with ATBN occurred in a solvent mixture of *N,N'*-dimethylsulfoxide, ethanol, and water. After this, the organophilic MMT was blended with acrylonitrile–butadiene rubber (NBR) by roll milling, and the rubber was vulcanized with sulfur. According to TEM observations, the silicate layers were well dispersed in the rubber matrix. The tensile stress at 100% elongation of this organoclay–rubber nanocomposite at 10 phr organoclay content was equal to that of a rubber containing 40 phr of carbon black. In this rubber–clay nanocomposite, the permeability of hydrogen and water decreased by 70% due to the incorporation of 3.9 vol.% organoclay.

Burnside and Giannelis presented the relationship between nanostructure and properties in polydimethylsiloxane–LS nanocomposites [24]. The solvent uptake in this “nanostructured” silicon rubber was dramatically decreased when compared to conventional composites. Both swelling behavior and modulus were related to the excess amount of bound rubber formed in the nanocomposites compared to the conventional composites.

The conditions for dispersing clay nanolayers into both *cis*-1,4-polyisoprene (IR) and epoxidized natural rubber (ENR) have been reported [25]. Incorporation of the clays into

these elastomers was achieved by mixing the components in an internal mixer/mixing mill (melt compounding) or by mixing their dispersions produced by toluene or methyl ethyl ketone solvents (solution intercalation). XRD studies indicated the intercalation of IR and ENR into the silicate interlayers, followed by exfoliation (delamination) of the silicate layers. The reinforcing effect strongly depended on the extent of dispersion of the silicate layers.

Solvent-assisted techniques may be important for the future as well. The reason behind this prediction is an interesting finding with melt compounded LS-reinforced, sulfur-cured rubbers. In such systems, considerable confinement (reaggregation) and even full deintercalation have been noticed [9,26,27]. This was believed to have been caused by chemical reactions in which the original surfactant of the OLS participated. The solvent-assisted techniques offer some possibilities to overcome the above problems observed in melt intercalation.

1.11 Applications

Polymer nanocomposites have several advantages for cryogenic storage tanks, specialty barrier packaging, spaceships, motor vehicles, etc. They are light weight, strong, and stiff; therefore, a smaller fraction of a vehicle's potential load capacity is used for propellant storage.

To obtain superior barrier properties, one should start with polymers that are good barriers, and adding nanodispersed clay can do further improvement of the materials. This approach has been examined by numerous companies. For example, Honeywell has commercialized its Aegis polymers that contain nanocomposites of nylon [28]. RTP Company, USA, has developed new nanoclay compounds designed to meet the stringent barrier demands in fuel system applications [29]. Nanocomposites perform exceptionally well in these fuel tank applications due to the high aspect ratio of the layers creating an extremely tortuous path for diffusion. The additive has a large aspect ratio that is key to the compound's unique properties – particularly barrier enhancement in which transmission rates can improve by two to four times. The improved permeation offered by the nanoclay compounds also provides benefits to applications in the food packaging industry. Nanoclay compounds reduce the amount of oxygen through the plastic packaging material used for fresh meats or other foods while simultaneously providing greater strength at the same thickness.

Nanoclay compounds offer improved mechanical and thermal properties compared to neat resins. Their low loading levels (2–8%) increase stiffness with minimal impact on specific gravity. Nanoclay compounds are ideal to be used in blow molding, injection molding, and blown film applications.

“In Mat” USA has commercialised nanocomposites' barrier coatings based on aqueous dispersions of polymers and exfoliated clays. Building on its first product line based on butyl elastomers, new nanocomposites coating formulations utilizing a variety of elastomers and nonelastomeric polymers have been made and characterized. Spray coating has been used in the tire and sporting goods industries, as it provides thickness control while enabling uniform coating to be applied to relatively complex shapes (e.g., tires and tennis ball). Dip coating is used to manufacture gloves and bladders for soccer balls. The flexible packaging industry typically uses high-speed roll coating in order to minimize the cost of applying large amounts of flexible packaging film.

References

1. Kickelbick, G., *Prog. Polym. Sci.*, 2003. **28**: p. 83.
2. Yoshida, M., M. Lal, N.D. Kumar, and P.N. Prasad, *J. Mater. Sci.*, 1997. **32**: p. 4047.
3. Pinnavaia, T.J., and G.W. Beall, *Polymer-Clay Nanocomposites*. 2001, Chichester, England: Wiley.
4. Friedrich, K., S. Fakirov, and Z. Zhang, *Polymer Composites – From Nano- to Macro Scale*. 2005, New York: Springer.
5. Schmidt, G., and M.M. Malwitz, *Curr. Opin. Colloid Interface Sci.*, 2003. **8**: p. 103.
6. Kojima, Y., A. Usuki, M. Kawasumi, Y. Fukushima, A. Okada, T. Kurauchi, and O. Kamigaito, *J. Mater. Res.*, 1993. **8**: p. 1185.
7. Vaia, R.A., and E.P. Giannelis, *Macromolecules*, 1997. **30**: p. 7990.
8. Vaia, R.A., and E.P. Giannelis, *Macromolecules*, 1997. **30**: p. 8000.
9. Varghese, S., and J. Karger-Kocsis, *J. Appl. Polym. Sci.*, 2004. **91**: p. 813.
10. Wang, D., J. Zhu, Q. Yao, and C.A. Wilkie, *Chem. Mater.*, 2002. **14**: p. 3837.
11. Neilson, L.E., *J. Macromol. Sci. (Chem.)*, 1967. **A1**(5): p. 929.
12. Okada, A., M. Kawasumi, A. Usuki, Y. Kojima, T. Kurauchi, and O. Kamigaito, *Mater. Res. Soc. Proc.*, 1990. **171**: p. 45.
13. Yano, K., A. Usuki, and A. Okada, *J. Polym. Sci. Part A: Polym. Chem.*, 1997. **35**: p. 2289.
14. Utracki, L.A., and R. Simha, *Macromolecules*, 2004. **37**: p. 10123.
15. Burnside, S.D., and E.P. Giannelis, *Chem. Mater.*, 1995. **5**: p. 1596.
16. Wang, W., Y. Li, L. Wei, and Y. Fang, *Mater. Lett.*, 2003. **57**: p. 3366.
17. Varghese, S., K.G. Gatos, A.A. Apostolov, and J. Karger-Kocsis, *J. Appl. Polym. Sci.*, 2004. **92**: p. 543.
18. Varghese, S., and J. Karger-Kocsis, *Polymer*, 2003. **44**: p. 4921.
19. Chen, Y., S. Zhou, and H. Yang, *J. Appl. Polym. Sci.*, 2005. **95**: p. 1032.
20. Wang, Y., H. Zhang, Y. Wu, J. Yang, and L. Zhang, *J. Appl. Polym. Sci.*, 2005. **96**: p. 318.
21. Wang, Y., H. Zhang, Y. Wu, J. Yang, and L. Zhang, *J. Appl. Polym. Sci.*, 2005. **96**: p. 324.
22. Ganter, M., W. Gronski, H. Semke, T. Zilg, C. Thomann, and R. Mulhaupt, *Kautschuk Gummi Kunststoffe*, 2001. **54**: p. 166.
23. Kojima, Y., K. Fukumori, A. Usuki, A. Okada, and T. Kurauchi, *J. Mater. Sci. Lett.*, 1993. **12**: p. 889.
24. Burnside, S.D., and E.P. Giannelis, *J. Polym. Sci. Part B: Polym. Phys.*, 2000. **38**: p. 1595.
25. Vu, Y.T., J.E. Mark, L.H. Pham, and M. Engelhardt, *J. Appl. Polym. Sci.*, 2001. **82**: p. 1391.
26. Gatos, K.G., R. Thomann, and J. Karger-Kocsis, *Polym. Int.*, 2004. **53**: p. 1191.
27. Sinha Ray, S., and M. Okamoto, *Prog. Polym. Sci.*, 2003. **28**: p. 1539.
28. Honeywell press release www.ageisnylon.com.
29. RTP company press release www.rtpcompany.com/news/press.

This page intentionally left blank

2 Polymer–Graphite Nanocomposites

*Sie Chin Tjong**

Department of Physics and Materials Science, City University of Hong Kong,
Tat Chee Avenue, Kowloon, Hong Kong

Abstract

This chapter provides a comprehensive overview on the structure, mechanical, electrical, and thermal characteristics of polymer–graphite nanocomposites. Inexpensive natural graphite exhibits a layered morphology with excellent electrical and thermal conductivities. The graphite layers can be intercalated with alkali metals followed by exfoliation with aqueous solvents. Alternatively, natural graphite can be converted to expanded graphite (EG) in which sulfuric acid is inserted between the carbon layers of graphite. When exposed to heat, exfoliation of the graphite occurs, yielding a dramatic expansion along the *c*-axis of the crystal structure by about three hundred times. In some cases, ultrasonication is used to separate loosely connected graphite nanosheets into individual nanoplatelets. Thin graphite nanoplatelets with large surface area and aspect ratio as well as high stiffness are ideal reinforcing fillers for conductive polymer nanocomposites. In general, only a small amount of expanded graphite ca. 0.74 vol.% is needed to reach the percolation threshold of transition in electrical conductivity for the conductive nanocomposites prepared from the PA6–graphite system. Introducing expanded graphite into PP markedly improves its flexural strength and stiffness as well as impact strength. However, expanded graphite addition enhances only the stiffness but not the tensile strength of epoxy resin owing to the formation of internal flaws during processing. The expanded graphite nanoplatelets are also beneficial in increasing the storage modulus of thermoplastics and thermosets. The glass transition temperature of such polymers tends to shift to higher temperatures due to the expanded graphite additions. The graphite nanoplatelets with high thermal conductivity are very effective to improve the conductivity of insulating polymers. Polymer–graphite nanocomposites are widely recognized as advanced functional materials with unique chemical, mechanical, and physical properties. They find applications as heat sinks in electronic packaging, antistatic media, shielding for electromagnetic or radio-frequency interference of electronic devices, biomedical sensors, and robotics.

2.1 Introduction

In recent years, there has been much interest in polymers reinforced by fillers of nanometer dimension because of their improved chemical, physical, and mechanical properties compared with neat polymers. The incorporation of nanofillers into polymers can significantly increase the tensile strength and stiffness, decrease gas permeability and flammability as well as enhance the thermal stability. The most interesting nanofillers include layered silicates, graphite nanoplatelets, inorganic nanoparticles, and carbon nanotubes (CNTs).

* Correspondence should be addressed to e-mail: aptjong@cityu.edu.hk

Among these nanofillers, graphite nanosheets and CNTs can further improve the electrical conductivity of polymer resins. Graphite is of particular interest because of its low cost and its ready availability. Conventional electrical conductive polymer composites reinforced with metal and carbon black particles have found widespread applications in industrial sectors such as materials for the electromagnetic interference shields, self-lubricated materials, etc. However, such microcomposites require rather high filler loading in order to achieve satisfactory electrical characteristics. This leads to poor processability and inferior mechanical performances of the microcomposites. In this regard, the incorporation of graphite nanoplatelets or nanosheets with large aspect ratio into insulating polymers can lead to the formation of nanocomposites with enhanced chemical, electrical, and thermal properties. The electrical conductivity is derived from the formation of continuous conduction paths in the composites. The critical filler content or percolation threshold needed to form conductive pathways in the polymer–graphite nanocomposites is relatively much smaller compared to that of the microcomposites. The properties of nanocomposites depend greatly on the chemistry of polymer matrices and the processing techniques such as *in situ* polymerization, solution, and melt intercalation. The dispersion of graphite nanoplatelets in the polymers is rather poor due to their large surface-to-volume ratio. The uniform dispersion of nanofillers in the polymer matrices is a general prerequisite for achieving desired chemical, mechanical, and physical characteristics.

2.2 Intercalated Compounds

Graphite is a polymorphic form of carbon. Its structure consists of graphene sheets stacked along the *c*-axis having a spacing of 0.335 nm (Figure 2.1). Each sheet contains hexagonal arrays of carbon atoms hybridized into sp^2 orbital forming sigma bonds with three coplanar neighbor atoms. Thus these bonds are strongly covalent. The graphite layers are formed from the aggregation of graphene sheets, held together by weak van der Waals forces. The space between the layers is referred to as “gallery” [1]. The weak interplanar forces allow for certain atoms, molecules, and ions to intercalate into galleries of the graphite aggregates. With the advances of materials synthesis and processing capabilities, graphite layers can be separated via intercalation and exfoliation. Therefore,

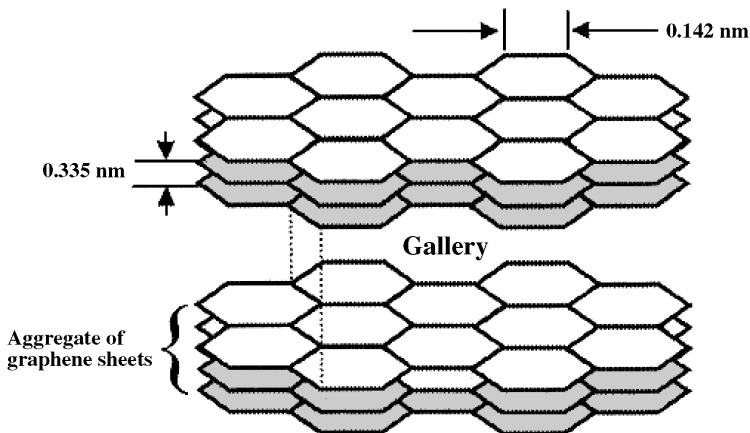
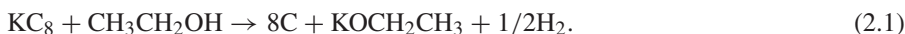


Figure 2.1. Schematic diagram of graphite layer structure.

thin nanoplatelets having a high surface area and aspect ratio as well as high stiffness can be formed. According to the literature, the theoretical surface area of graphite sheet is 2965 m²/g [2] and theoretical Young's modulus of an individual graphite sheet is 1060 GPa [3]. Graphite nanosheets can be prepared either via the chemical methods based on intercalation of graphite followed by thermal annealing or by a mechanical milling. In the latter route, extensive plastic deformation induces structural changes and crystalline size reductions in graphite during mechanical milling. More recently, Vittori Antisari et al. demonstrated that the graphite nanosheets with a thickness of ~10 nm can be obtained by grinding graphite powder under low energy pure shear milling using water as a lubricant [4].

Intercalation of guest species into layered inorganic materials is an effective route of producing inorganic–organic nanocomposites with unique microstructures controlled by host–guest and guest–guest interactions. Layered materials like clay silicates are hydrophilic. Intercalation of organic surfactant molecules into the clay galleries through ion exchange reactions with sodium cations leads to the formation of organoclays. Nanocomposites are formed when a small amount of organoclays is incorporated into polymers. The conversion of hydrophilic inorganic clays to a hydrophobic organoclays improves the interfacial adhesion between the organic and inorganic phases when a hydrophobic polymer matrix is involved. Depending on the structure of dispersed clay platelets in the polymer matrix, the composites can be classified as intercalated or exfoliated nanocomposites. Intercalated structures are self-assembled, well-ordered multilayered structures where the extended polymer chains are inserted into the gallery space of the clays. This leads to an expansion of the interlayer spacing. In an exfoliated structure, individual silicate sheets are delaminated, and dispersed as nanoscale platelets in a polymer matrix. Since graphite does not have alkali cations in its galleries and net charge on its surfaces, ion exchange reactions with organic surfactants are unlikely to occur. However, graphite is known to form intercalated compounds (GIC) by exposing it to appropriate atoms or molecules, known as the intercalant that enter the interplanar layers of the graphite [5]. GIC can be synthesized from the electron-donor agents, e.g., reducing agents such as alkali metals and the electron acceptors, e.g., oxidizing agents such as halogens and oxacids. In the GICs, carbon layers and intercalated layers are stacked in a periodic mode, often referred to as “staging.” The stacking can be of the types of stage 1, 2, 3, or *n*, depending on the intercalating conditions and guest species (Figure 2.2). To achieve thin graphite platelets, the stage of GIC must be kept to be as small as possible.

Alkali metals such as potassium can be inserted into the graphite interplanar spacings and galleries to yield a number of compounds [6,7]. The first stage intercalation compound, KC₈, has a larger *d*-spacing (5.41 Å) compared to that of graphite. Second stage compound, KC₂₄, and the third stage material, KC₃₆, have a spacing of 8.72 and 12.1 Å, respectively. Viculis et al. [8] reported that KC₈ could be readily formed by heating graphite powder with potassium metal under vacuum at 200 °C. The KC₈ compound can be further exfoliated in aqueous solvent (e.g., ethanol) to produce graphite nanoplatelets of 40 layers thick via the following reaction:



Solvation of potassium ions, along with hydrogen gas evolution, assists in separating the graphitic layers. The resulting dispersion is basis due to the formation of potassium ethoxide. It is washed several times until a neutral pH is obtained. A schematic diagram showing the intercalation/exfoliation of graphite is shown in Figure 2.3.

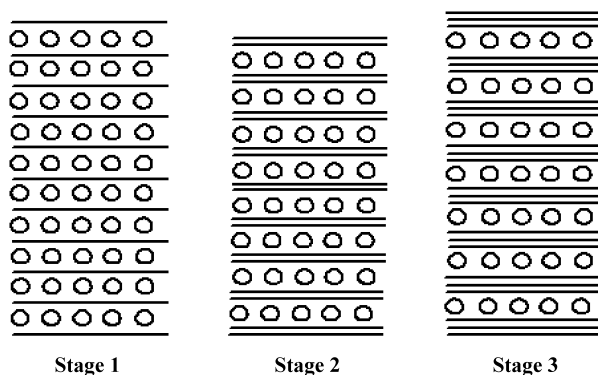


Figure 2.2. Schematic diagram of stage 1, 2, and 3 GICs. (—) Graphene layer and (○) intercalated species.

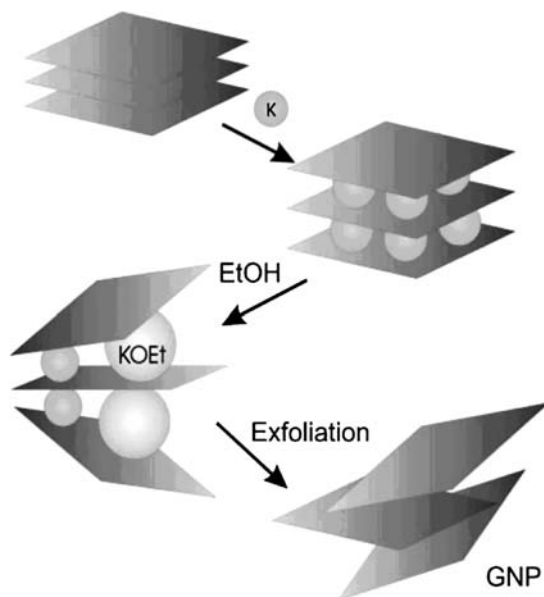


Figure 2.3. Schematic diagram of the intercalation/exfoliation process. Graphite is intercalated with potassium metal and then exfoliated with ethanol to form a dispersion of carbon nanoplatelets. Reprinted from [8] with permission of AAAS.

Shioyama reported that unsaturated carbons could be co-intercalated into the graphite layers of KC_8 or KC_{24} [7]. Polymerization reaction takes place between alkali metal–GICs and the vapor of liquid hydrocarbons of isoprene, 1,3-butadiene, and styrene after several tens of minutes of contact. The potassium–GIC acts as an initiator for the polymerization. X-ray diffraction pattern of the polymers displays no reflections for graphite or GIC, indicating that the graphite layers are delaminated by hydrocarbon molecules during polymerization. A schematic diagram showing the GIC-initiated polymerization with unsaturated hydrocarbon is depicted in Figure 2.4. Using a similar approach, Sun et al. reported the synthesis of polystyrene (PS)–graphite nanocomposite using potassium–

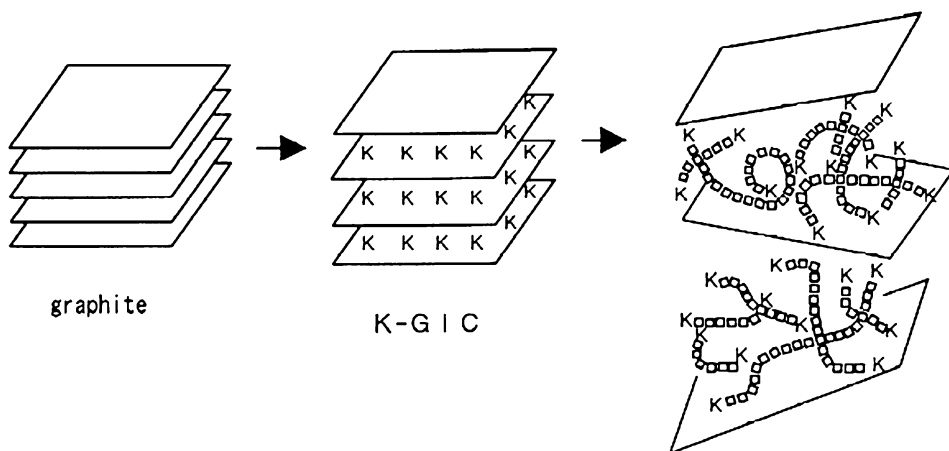


Figure 2.4. Schematic diagram showing the GIC-initiated polymerization: (K) potassium and (□) unsaturated carbon. Reprinted from [7] with permission of Elsevier.

tetrahydrofuran–GIC as an initiator. The polymerization mainly occurred at the surface and edge of graphite [9].

For practical industrial applications, intercalation compound such as graphite oxide (GO) can be prepared via oxidation of graphite in sulfuric acid in the presence of an oxidizing agent such as nitric acid. Other environment employed includes the $\text{H}_2\text{SO}_4/\text{KMnO}_4$ solution [10–15]. A typical reaction between graphite in the $\text{H}_2\text{SO}_4/\text{HNO}_3$ (4:1 volume ratio) solution is given as follows [16]:



where (O) is oxidant and ($\text{graphite} \cdot \text{HSO}_4$) is GIC. In this process, nitric acid serves as an oxidizer and sulfuric acid as an intercalant. The GIC is then exposed to thermal atmosphere to release the acid, leading to the formation of the so-called expanded graphite (EG). In some cases, it is followed by ultrasonication treatment to separate the loosely connected graphite nanosheets into individual nanosheets. During rapid heating in a furnace at 900–1000 °C, the intercalant decomposes and forces the graphite layers to delaminate. This results in an expansion in the c -direction of EG about 300 times that of original graphite [17]. Microwave, infrared, or laser irradiation can also be used as an alternative source to perform rapid heating for GIC [18].

Figures 2.5a and b show low magnification SEM micrographs of the EG. Apparently, EG appears as a loose, porous, vermicular or worm-like material having numerous delaminated nanosheets that constitute a network with pores of different sizes. The thickness of individual graphite sheet in EG is ~ 100 nm [19,20]. After sonication, the graphite sheets of EG are further dispersed into nanosheets with thickness of ~ 30 – 80 nm and diameter of ~ 0.5 – 20 μm (Figure 2.6). Higher magnification of TEM micrograph reveals that the graphite nanosheet consists of thinner nanolamellae with thickness of 1–5 nm or even thinner (Figure 2.7). The mean particle size (diameter) of sonicated EG depends considerably on the ultrasonic irradiation times (Figure 2.8). The particle size decreases sharply during the early stage of irradiation up to 10 h. The graphite nanosheets of sonicated EG subjected to 10 h irradiation exhibit a thickness of 52 nm and a size of 13 μm . These

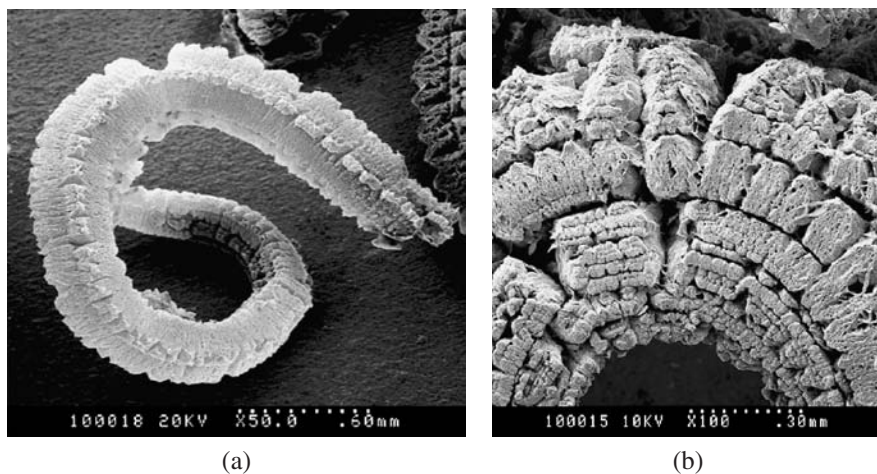


Figure 2.5. SEM micrographs showing (a) worm-like morphology and (b) porous nature of expanded graphite (EG) at very low magnifications. Reprinted from [18] with permission of Elsevier.

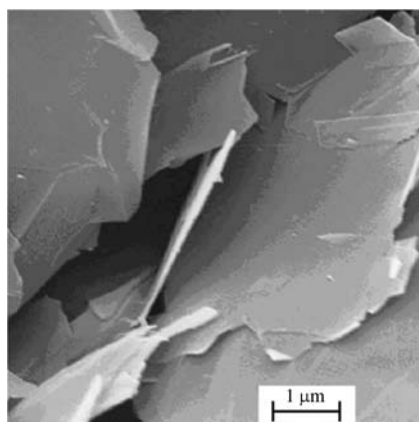


Figure 2.6. SEM micrograph of sonicated expanded graphite. Reprinted from [20] with permission of Elsevier.

dimensions correspond to a large aspect ratio (width-to-thickness) of ~ 250 . Prolonged ultrasonic treatment of EG above 10 h would not further reduce its particle sizes [21]. As mentioned above, the GIC exhibits a layer-stacking structure in which the thickness of the nanosheets in exfoliated graphite could be as thin as a single carbon layer when the precursor is stage 1 GIC. The GICs prepared from chemical oxidation route are mostly confined to stage 1 to stage 5. Therefore, the thickness of the sheets is within about 1–2.5 nm, assuming the thickness of single carbon layer is 0.5 nm [20].

More recently, Kaner and co-workers synthesized graphite nanoplatelets with thicknesses down to 2–10 nm by alkali metal intercalation followed by ethanol exfoliation and microwave heating [22]. In the synthesis process, graphite that has already been intercalated and exfoliated with a mixture of nitric and sulfuric acid is reintercalated with an alkali metal (e.g., potassium) at 200 °C to form a first stage compound. Further reaction of the intercalated graphite with ethanol causes exfoliation of the graphene layers as

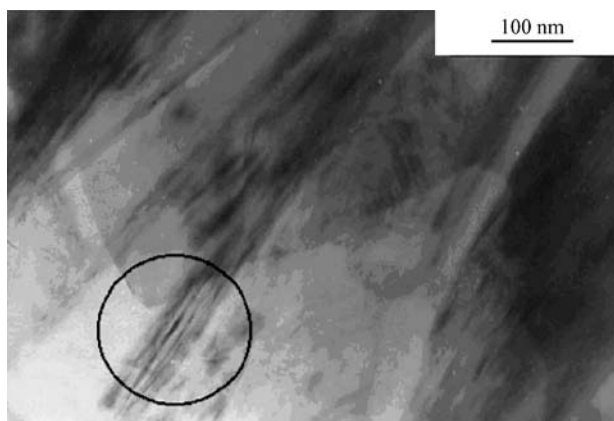


Figure 2.7. TEM micrograph showing thinner nanosheets of expanded graphite. Reprinted from [20] with permission of Elsevier.

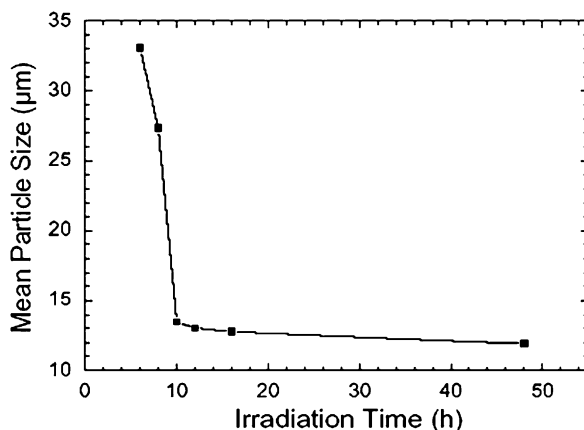


Figure 2.8. Mean particle size vs. ultrasonic irradiation time for EG subjected to sonication treatment. Reprinted from [21] with permission of Elsevier.

given by reaction (2.1). Figure 2.9b shows the SEM micrograph of EG after reintercalation with potassium and exfoliation with ethanol. For the purpose of comparison, the SEM micrograph of starting graphite is also shown (Figure 2.9a). Microwave treatment of the exfoliated platelets assists in removal of trapped solvent, thereby causing a further expansion of the platelets with thicknesses down to 10 nm.

Generally, GO has a large number of polar groups on the edges of graphite layers, such as carbonyl and carboxyl, as well as the epoxide and hydroxyl groups within the basal planes of the graphene sheets [10]. These oxygen functional groups alter the van der Waals interactions between the layers of graphite oxide and render them hydrophilic. This facilitates their hydration and exfoliation in aqueous media. In this case, intercalation of water-soluble polymers such as poly(ethylene oxide) and poly(vinyl alcohol) (PVA) in GO can occur [13–15]. Thus, the EG products are simply added to aqueous solution of the polymers to form the graphite–polymer nanocomposites. Figure 2.10 shows the

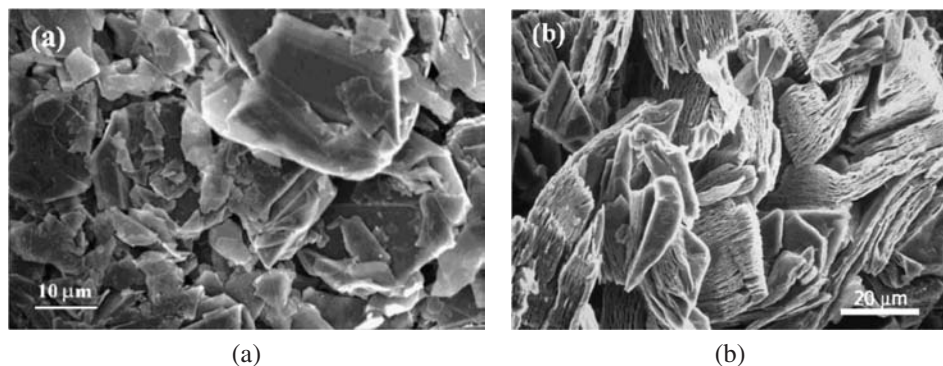


Figure 2.9. SEM photographs of (a) starting graphite and (b) after intercalation with potassium and exfoliation with ethanol. Reprinted from [22] with permission from The Royal Society of Chemistry.

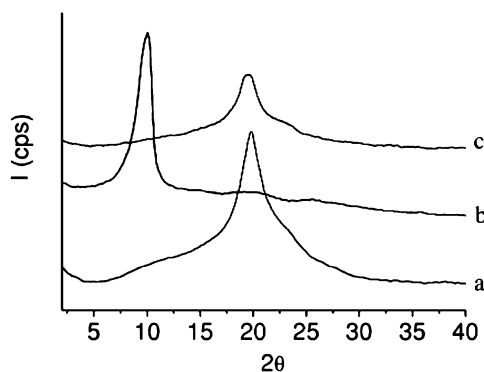


Figure 2.10. XRD patterns of (a) PVA, (b) GO, and (c) PVA-GO nanocomposite. Reprinted from [15] with permission of Elsevier.

typical X-ray diffraction (XRD) patterns of PVA, GO, and graphite-PVA nanocomposite specimens. The characteristic diffraction peak of GO is located at about $2\theta = 10^\circ$, corresponding to the d -spacing of 0.88 nm. After reacting with PVA to form the nanocomposite, the characteristic diffraction peak of GO disappears, and only the diffraction peak of PVA at $2\theta = 21^\circ$ is observed. This implies that the layered stacking structure of GO is destroyed and the GO sheets are delaminated. X-ray diffraction is a powerful tool to characterize the structure of polymer nanocomposites. For an intercalated structure, the characteristic peak of GO would shift to lower angle regime due to the expansion of the basal spacing. In contrast, no peaks are observed in the XRD pattern of exfoliated polymer nanocomposites due to loss of the structural registry of the layers. The absence of Bragg diffraction peaks in the nanocomposites may indicate that the graphite sheets have been completely delaminated or disordered. Further transmission electron microscopic (TEM) observation is needed to verify the formation of an exfoliated structure. Figure 2.11 shows the TEM image of the PVA-GO nanocomposite. This figure reveals a homogeneous dispersion of exfoliated graphite nanosheets in the PVA matrix. It is noted that the presence of $-OH$ and $-COOH$ functional groups in GO facilitate chemical interactions between the polymer molecules and graphite nanosheets. Consequently, suitable monomers, initiators,

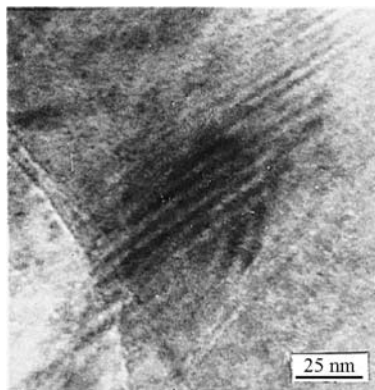


Figure 2.11. TEM micrograph of PVA–GO nanocomposite. Reprinted from [15] with permission of Elsevier.

and macromolecules are capable to intercalate into the galleries and pores of EG under proper processing conditions to form the nanocomposites.

2.3 Synthesis of Nanocomposites with Thermoplastic Matrices

2.3.1 *In situ* Polymerization

The high surface area of graphite nanosheets and porous structure of EG favor *in situ* polymerization of polymer–graphite nanocomposites. This process involves inserting a monomer into the pores of EG through physical adsorption and then expanding the graphite layers into the matrix by polymerization. Several nanocomposites have been successfully synthesized via *in situ* polymerization. These include PA6–graphite [23,24], polystyrene–graphite [25–27], poly(methyl methacrylate) (PMMA)–graphite [28–30], poly(arylene disulfide)–graphite [31], and unsaturated polyester–graphite [32]. For example, Pan et al. prepared the PA6–graphite nanocomposites by *in situ* intercalative polymerization of ϵ -caprolactam with EG in the presence of a small amount of aminocaproic acid catalyst [23]. In this process, the ϵ -caprolactam monomer and catalyst were intercalated into the galleries and pores of EG via polar interaction between ϵ -caprolactam with the –OH and –COOH functional groups of EG. The carboxyl end groups initiated ring-opening polymerization of ϵ -caprolactam with the aid of catalyst at 180–240 °C. TEM examination reveals that the graphite sheets of the PA6–graphite nanocomposites are exfoliated into platelets with thickness of about 10 nm. The nanocomposites exhibit improvements in electrical conductivity. Ping and Yuan synthesized the PMMA–graphite nanocomposites by emulsion polymerization of methyl methacrylate (MMA) in the presence of GO [30]. MMA is a polar monomer and can be intercalated into GO via the polar interaction between MMA molecules and polar groups on the surface of GO-layered sheets.

Chen et al. prepared polystyrene–graphite material by *in situ* polymerization of polar MMA monomer with EG in the presence of benzoyl peroxide (BPO). The composite was used as a precursor to prepare the poly(vinyl chloride)/PMMA–graphite nanocomposite [28]. Recently, they employed ultrasonic vibration during polymerization to further disperse graphite sheets within the polymer matrix [29]. The nanocomposites were then dispersed to chloroform (CHCl₃) and cast on the glass slides to form conducting films.

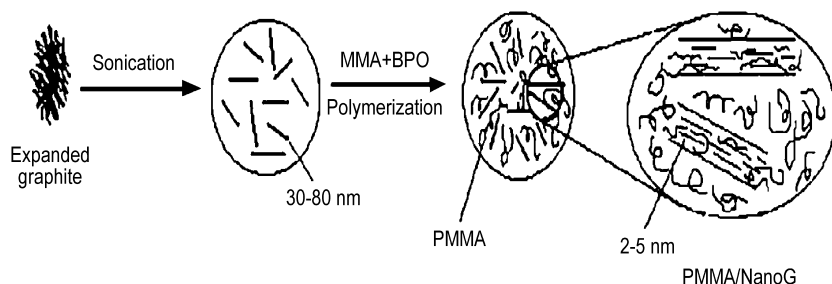


Figure 2.12. Schematic illustration showing *in situ* polymerization of PMMA–graphite nanocomposite aided by sonication. Reprinted from [29] with permission of Elsevier.

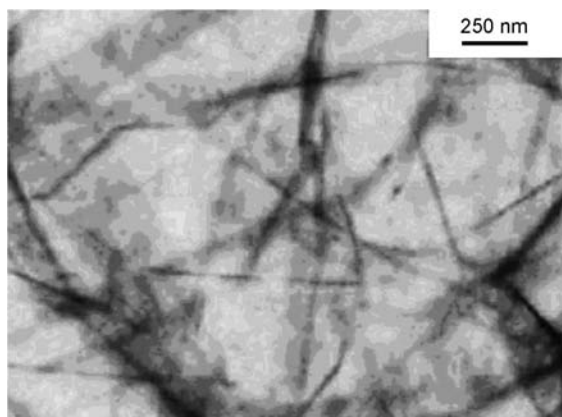


Figure 2.13. TEM micrograph of *in situ* polymerized PMMA–graphite nanocomposite showing random dispersion of graphite nanoplatelets with large aspect ratio. Reprinted from [29] with permission of Elsevier.

The polymerization procedures are summarized in schematic diagrams as shown in Figure 2.12. Using this procedure, graphite nanoplatelets with thickness ranging from 30 to 80 nm are randomly distributed within the polymer matrix, facilitating the formation of effective conductive network (Figure 2.13).

2.3.2 Solution Intercalation

In solution route, GO and the polymer are mixed and dispersed in an adequate organic solvent. The polymer dissolves in the solvent then adsorbs onto the expanded graphite sheets. Porous EG having –OH and –COOH functional groups facilitates physical and chemical adsorption between the EG and polymer solution. When the solvent is evaporated, the graphite sheets reassemble, sandwiching the polymer to form the nanocomposites. Zheng and Wong have successfully prepared the PMMA–graphite nanocomposites via the solution blending method [19]. In the process, dried PMMA pellets were dissolved into solution with chloroform and then mixed with EG fillers in different weight fractions in a flask by stirring aided by a sonicator. The solvent was finally evaporated at 60 °C.

For polyolefin polymers containing no polar groups in their backbones, the intercalation of polyolefin molecular chains into EG is rather difficult. The polar groups such as vinyl-functionalized polar olefins (methyl acrylate, acrylonitrile) can be incorporated into

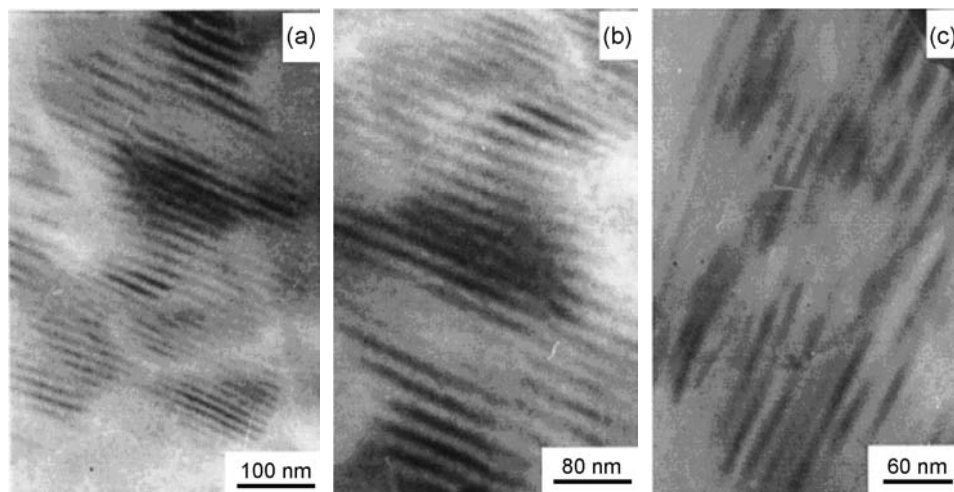


Figure 2.14. TEM micrographs showing the dispersion of graphite nanosheets in maleated PE–graphite nanocomposite with 3.96% filler prepared by (a and b) solution intercalation and (c) masterbatch melt mixing. Reprinted from [34] with permission of Wiley.

a linear polyethylene (PE) backbone. Very recently, Cerezo et al. used poly(ethylene-*co*-methyl acrylate-*co*-acrylic acid) terpolymer (EMMA) as the host matrix for the nanocomposite due to its enhanced compatibility with GO [33]. In this respect, polar interaction between the polar host polymer and the –OH and –COOH facilitates the formation of nanocomposite during solution blending. In another approach, maleic anhydride (MA) functional group is grafted to polyolefins prior to the solution intercalation. Shen et al. prepared the maleated polypropylene (PP)–graphite and maleated polyethylene (PE)–graphite nanocomposite via the solution intercalation and melt mixing processes using the MA-*g*-PP or MA-*g*-PE compatibilizer [34]. During solution processing, the MA-*g*-polyolefin molecules can more easily intercalate into the pores and galleries of EG through physical adsorption and polar interaction between the MA functional group of polyolefins with the –OH and –COOH groups of EG. Typical TEM micrographs of the maleated PE–graphite nanocomposites prepared via solution intercalation process reveal that the graphite sheets are exfoliated into nanoplatelets with thickness and interlayer spacing of about 10 nm and parallel to each other (Figures 2.14a and b). Thus, the dispersed graphite nanosheets have a high aspect ratio (width-to-thickness) of more than 30. In contrast, the graphite nanosheets of maleated PE–graphite nanocomposites prepared via melt intercalation exhibit nonuniform thickness and interlayer spacing. The exfoliated nanosheets have lower aspect ratio accordingly (Figure 2.14c).

2.3.3 Melt Intercalation

For commercial production of graphite–polymer nanocomposites, *in situ* polymerization and solution intercalation routes are ineffective due to the high cost of monomers and environmental issue of the organic solvents. However, melt compounding is a versatile commercial process capable of producing a variety of polymer products on large volume scales. It is considered the most cost-effective route to prepare the polymer nanocomposites due to its flexibility and compatibility with current industrial processing facilities

such as extruder and injection molder. Melt compounding involves mixing of the EG with polymer pellets, and heating the mixtures above the melt temperature of polymers in an extruder or mixer. Several nanocomposite systems such as maleated PP–graphite, maleated PE–graphite, PS–graphite, and PA6–graphite have been successfully prepared by melt compounding [1,26,34,35].

2.4 Synthesis of Nanocomposites with Thermoset Matrices

Epoxy is a family of thermosets having good electrical insulation, desirable mechanical behavior, and excellent chemical and thermal stability. Therefore, epoxy resins find wide applications in industrial sectors ranging from matrix materials of polymer composites to adhesives. To form solid thermosetting materials, a low molecular weight prepolymer is cured with cross-linking agents and/or catalysts. During curing, chemical and structural changes occur on a molecular level, leading to the formation of a cross-linked network structure. Generally, diglycidyl ether of bisphenol A (DGEBA; Epon 828) is commonly used as the matrix for polymer nanocomposite. The Epon 828 was developed by Shell Chemical from a reaction of bisphenol with epichlorohydrin to yield a compound containing about two epoxy functional groups per molecule. The epoxy polymerization is initiated by organic basic agents such as amines or anhydrides and the reaction is exothermic. It requires heating to reach completion in a desired time period. The epoxy resins are brittle in nature because of their cross-linked molecular structures. Consequently, they have poor resistance to crack initiation and growth.

Comparing to the graphite–thermoplastic nanocomposites, less information is available on the synthesis, electrical, and mechanical behavior of the graphite–epoxy (Epon 828) nanocomposites. Li et al. studied the effect of UV/ozone treatment of sonicated EG graphite on the synthesis and electrical behavior of the epoxy–graphite nanocomposites [36]. The EG particles were sonicated for 2 and 8 h, respectively, prior to curing of the epoxy resin with 1,3-phenylenediamine. The mean particle size and the extent exfoliation of EG depend considerably on ultrasonic irradiation times. Figures 2.15a and b show the morphologies of graphite–epoxy nanocomposites reinforced with 2 wt.% EG sonicated

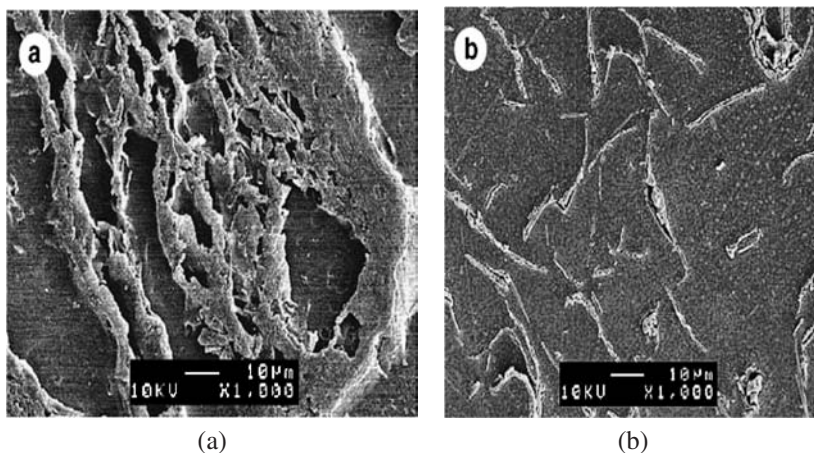
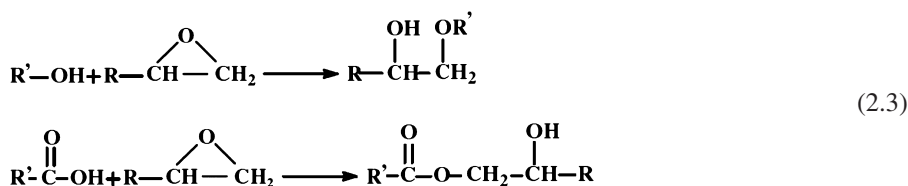


Figure 2.15. SEM micrographs of epoxy–graphite nanocomposites reinforced with 2 wt.% EG sonicated for (a) 2 h and (b) 8 h prior to epoxy curing. Reprinted from [36] with permission of Elsevier.

for 2 and 8 h. It can be seen that the EGs sonicated for 2 h exhibit porous structure as expected. However, the EGs sonicated for 8 h are well dispersed and exfoliated in the epoxy matrix. Moreover, UV/ozone treatment induces formation of the hydroxyl and carboxyl functional groups on the EG surface via oxidation process. Such functional groups are reactive to epoxy, which form strong chemical bonds with epoxy and enhance the graphite–epoxy adhesions [37]. Typical chemical reactions between the hydroxyl and carboxyl functional groups on the graphite nanoplatelets and epoxy resins can be described by the following chemical reactions:



where R' is the hydrocarbon radical containing carbon atom in the graphite nanoplatelets.

More recently, Daniel and co-workers used several processing techniques such as direct sonication, shear and combined sonication, and shear mixing techniques to prepare the epoxy–graphite nanocomposites [38,39]. Figure 2.16 shows a flowchart for the preparation of nanocomposites using these techniques. The morphologies of epoxy–graphite (1%) nanocomposite specimens prepared from different processing techniques are shown in Figures 2.17a–d. From Figure 2.17a, large EG particles are distributed nonuniformly in the epoxy matrix prepared from direct mixing route. In contrast, other processing techniques are more effective to disperse EG uniformly into finer particles, particularly those prepared from combined sonication and shear mixing (Figure 2.17d).

Karner and co-workers prepared the graphite–epoxy nanocomposites using the GIC in which the intercalants are sulfuric acid and potassium as discussed above. Such GICs were dispersed into an Epon 862 amine cured epoxy resin matrix [40]. Moreover, a covalent linkage between the resin molecules and the graphite nanosheets can be established by grafting an amine or carboxylic acid functional groups on the fringes of the graphite nanosheets.

2.5 Synthesis of Nanocomposites with Rubber Matrices

Flexible conductive rubbers have been a subject of interest for many years. Various rubbers, e.g., silicone rubber (SR), acrylonitrile butadiene rubber (NBR), natural rubber, and ethylene propylene diene rubber (EPDM) are used for preparation of such microcomposites [41]. In particular, SR with excellent elastic, thermal, and mechanical properties has been widely used as the matrix material for polymer microcomposites for desirable applications. For example, the coupling of mechanical and electrical properties (piezoresistance) allows the silicone–graphite microcomposites to perform as a continuous load transducer with application to fields of biomedical engineering and robotics [42]. Because of the high aspect ratio of the graphite nanoplatelets, a novel finger-sensing nanocomposite with remarkable piezoresistivity has been successfully synthesized by dispersing graphite nanofillers in a SR matrix via solution blending process [43]. Recently, nanocomposites of NBR and EG have been synthesized by melt mixing [44,45].

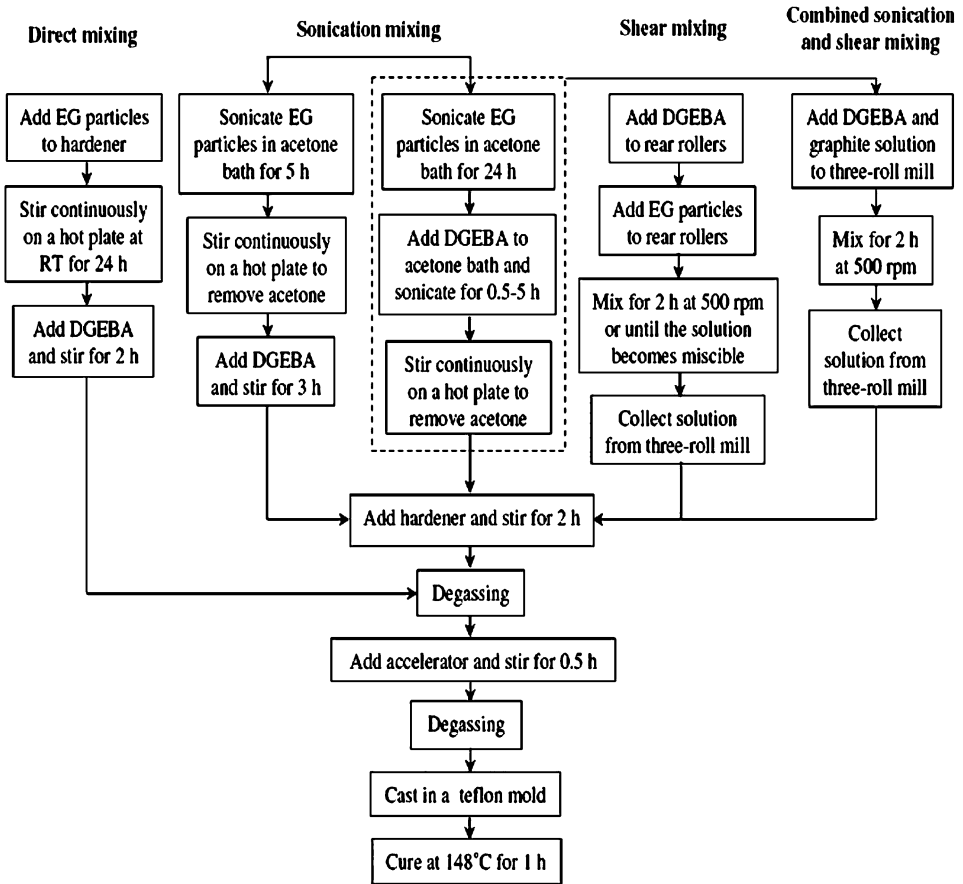


Figure 2.16. Flowchart of processing techniques for preparing the epoxy-graphite nanocomposites. Reprinted from [39] with permission of Elsevier.

2.6 Mechanical Characteristics

The mechanical properties of polymer-graphite nanocomposites are strongly related to the extent of exfoliation and dispersion of graphite platelets in the polymer matrix. The graphite nanosheets with high aspect ratios enable an effective stress transfer for the nanocomposites during mechanical loading. The theoretical Young's modulus of an individual graphite sheet is 1060 GPa, which is much higher than that of clay platelet (~ 170 GPa). Graphite nanosheets with high stiffness and aspect ratio offer a great potential for upgrading the mechanical performances of polymers. Unfortunately, stiffening and strengthening effects of graphite nanoplatelets are far from ideal. Some polymer-graphite nanocomposites are found to exhibit inferior mechanical performances due to induced internal flaws in these materials and degradation of the host polymers during processing. An exceptionally high stiffness of the nanocomposites has been observed in the form of composite nanofibers only. It is recognized that the mechanical properties of polymer fibers can increase dramatically by reducing their diameters as a result of the decreased probability of surface and internal flaws. Mack et al. employed electrospinning to study the elastic

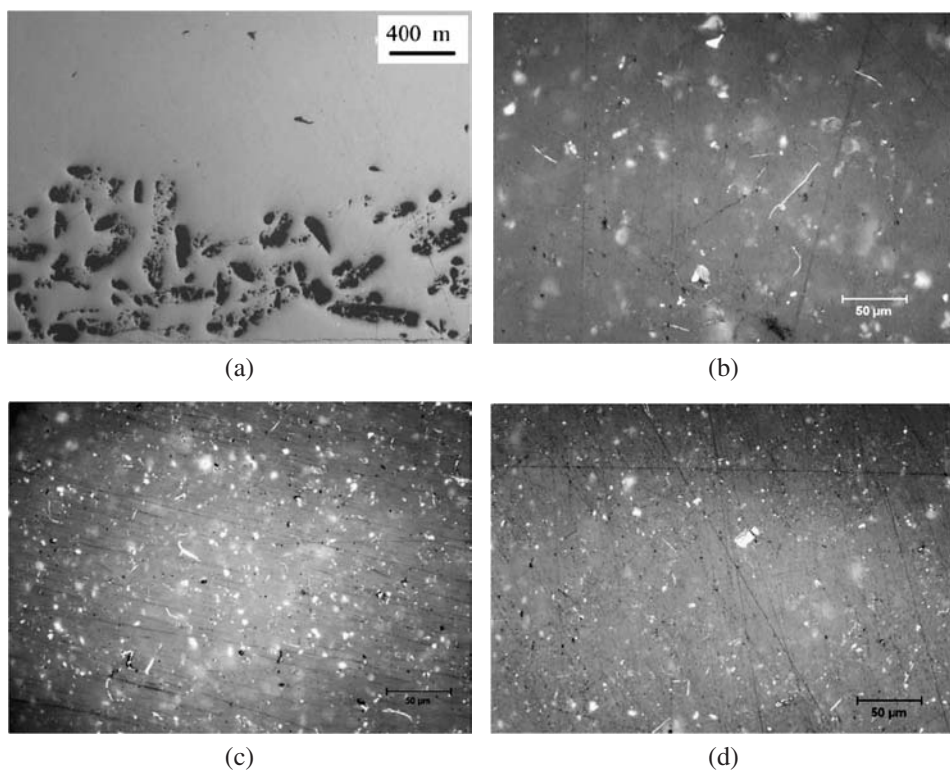
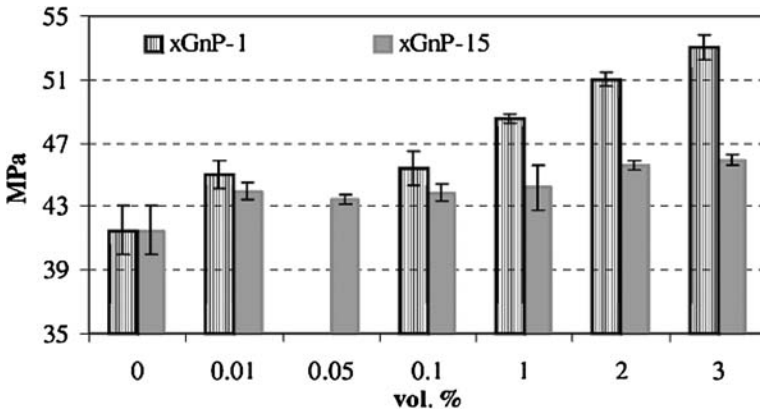


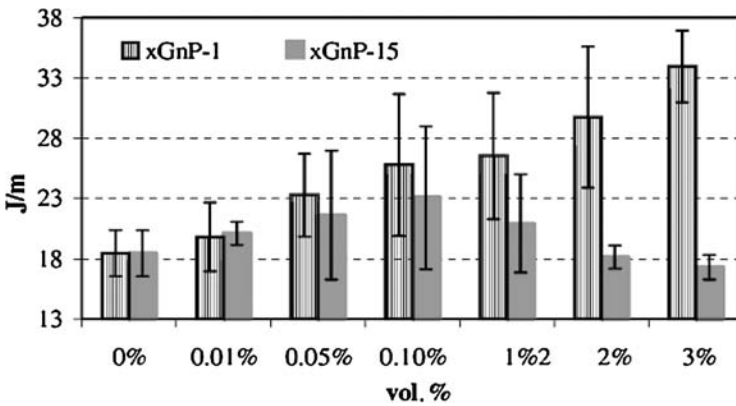
Figure 2.17. Optical micrographs showing the morphologies of epoxy–graphite nanocomposite specimens prepared by (a) direct mixing, (b) sonication mixing, (c) shear mixing, and (d) combined mixing. Reprinted from [39] with permission of Elsevier.

properties of polyacrylonitrile (PAN)–graphite nanocomposite fibers [46]. The nanocomposite fibers were prepared by adding 1–4 wt.% graphite nanoplatelets to a PAN solution containing *N,N*-dimethylformamide. They reported that additions of very small amount of graphite nanoplatelets (1–4 wt.%) could produce the largest modulus enhancement for PAN. The modulus stiffening effect of graphite nanosheets in PAN nanocomposite fibers is almost comparable with that of the carbon nanotube-reinforced PAN counterparts.

Porous EG is considered to have good compatibility with both polar and nonpolar polymers owing to its polar hydroxyl and carboxyl functional groups can interact with the host polymers. For polar PA6, EG additions are found to degrade the tensile strength and modulus of PA6 due to the release of sulfuric acid from EG during melt compounding [35]. Therefore, acid instability of PA6 contributes to poorer mechanical performances of the PA6–graphite nanocomposites. For nonpolar polyolefins, Kalaitzidou et al. reported that EG addition is beneficial in improving the flexural strength, stiffness, and impact strength of nonpolar PP polymer [47]. In their study, exfoliated graphite platelets of less than 10 nm thick and a diameter of $\sim 15 \mu\text{m}$ (denoted as xGnP-15) were produced by immersing graphite in a sulfuric-acid-based solution, followed by heating and ultrasonic treatments. The diameter can be further reduced by using a vibratory mill, resulting in nanoplatelets with the same thickness but with diameter less than $1 \mu\text{m}$ (denoted as xGnP-1). The flexural strength and impact strength of both the PP-xGnP-1 and PP-xGnP-15 nanocomposites



(a)



(b)

Figure 2.18. (a) Flexural strength and (b) impact strength of PP-xGnP-1 and PP-xGnP-15 nanocomposites. Reprinted from [47] with permission of Elsevier.

at low loading levels are shown in Figures 2.18a and b, respectively. It is apparent that the xGnP-1 is more effective as reinforcement for PP. They attributed such an improvement in tensile strength to a better dispersion of graphite nanoplatelets in polymer matrix at low loading levels. The enhancement in impact strength possibly results from the formation of finer spherulites as a result of graphite addition. Similar beneficial reinforcing and stiffening effects have also been observed in the polyethylene-graphite nanocomposites [48,49].

In the case of the epoxy-graphite nanocomposites, Daniel and co-workers demonstrated that the processing routes have a large influence on the tensile properties of nanocomposites [39]. Figure 2.19 shows the stress-strain curves for pure epoxy and its nanocomposites prepared by several processing techniques. Young's moduli of the epoxy-graphite (1 wt.%) nanocomposite specimens processed by different techniques are shown in Figure 2.20. It is apparent that all nanocomposite specimens exhibit higher modulus than neat epoxy, but they have much lower tensile strength and strain than pure epoxy, particularly those prepared via direct mixing process. The lower tensile strength of nanocomposites is attributed to a weak interfacial bonding between graphite nanosheet

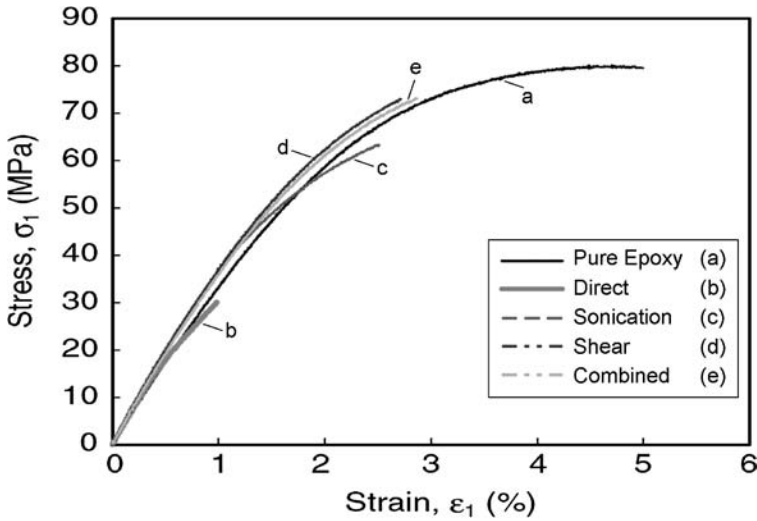


Figure 2.19. Tensile stress–strain behavior of pure epoxy and its nanocomposites reinforced with 1 wt.% EG processed by different techniques. Reprinted and amended from [39] with permission of Elsevier.

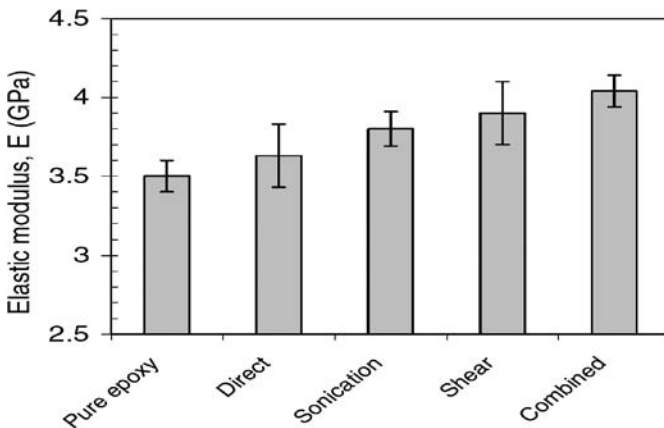


Figure 2.20. Elastic moduli of epoxy–graphite (1 wt.% EG) nanocomposites prepared by different processing techniques. Reprinted from [39] with permission of Elsevier.

and epoxy matrix and to the formation of internal flaws during curing. The tensile behavior of the epoxy–graphite nanocomposites is somewhat similar to that of the epoxy–clay nanocomposites prepared by the so-called slurry compounding process (Figure 2.21) [50]. However, epoxy–clay nanocomposites exhibit much higher fracture toughness than the neat epoxy due to the clay nanoplatelets that can effectively deflect the propagation of microcracks into tortuous paths. More recently, Schulte and co-workers reported that the epoxy nanocomposites reinforced with 0.3 wt.% double-walled carbon nanotubes (DWNTs) exhibit higher ultimate tensile strength and strain to failure, particularly for the amino-functionalized DWNT [51]. This is due to a very large aspect ratio of carbon nanotubes compared to that of graphite nanoplatelets. Carbon nanotubes are known to possess a very large aspect ratio of ~ 1000 [52]. In this respect, the CNTs are very effective to

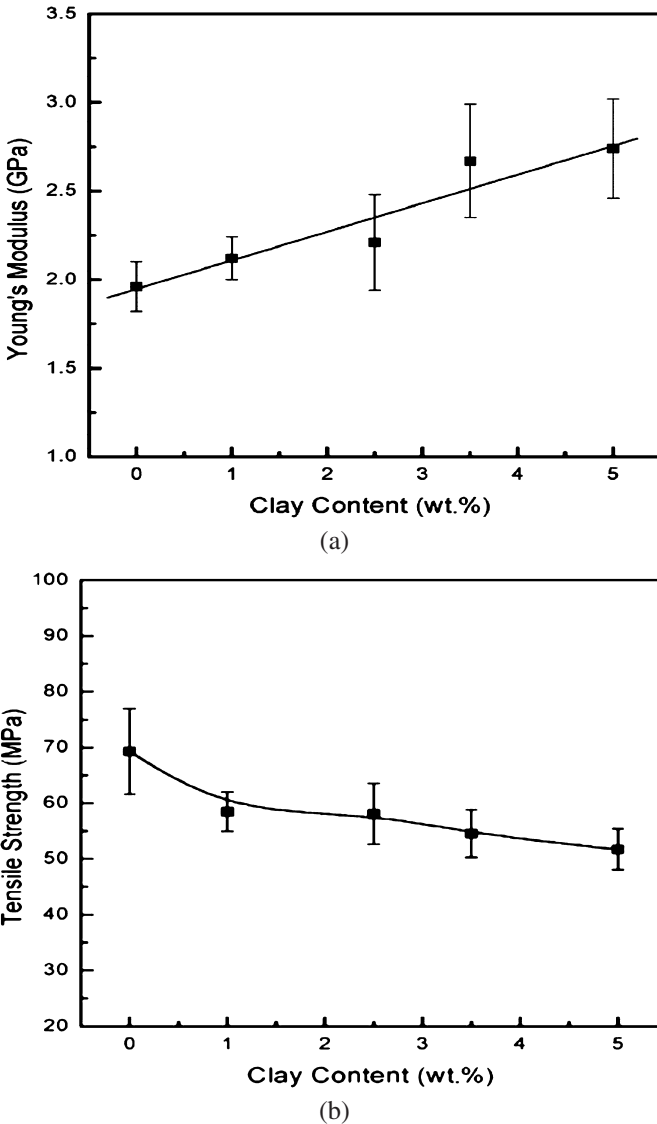


Figure 2.21. (a) Young's modulus and (b) tensile strength vs. clay content for the epoxy-clay nanocomposites. Reprinted from [50] with permission from The American Chemical Society.

bridge the microcracks and pores in the epoxy matrix during tensile deformation, thereby enhancing the tensile strength and ductility of the nanocomposites. It is anticipated that graphite nanoplatelets with large aspect ratios can also bridge the cracks in brittle epoxy resins provided that proper processing and curing are adopted. More works in near future are needed to elucidate this issue.

The thermomechanical behavior of the polymer-graphite nanocomposites is now considered. Dynamical mechanical analysis (DMA) over a wide temperature range is widely recognized as a powerful tool to evaluate the viscoelastic behavior of polymer nanocomposites. Several important parameters such as storage modulus (E'), loss mod-

ulus (E''), and loss tangent ($\tan \delta$) can be retrieved from the DMA measurements. The peak maximum of E'' or $\tan \delta$ is an indicator of the glass transition (T_g), which is the viscoelastic transition of a material. Very recently, Shanks and co-workers demonstrated that the incorporation of EG into PP-*g*-MA enhances its storage modulus considerably, due to the hydrogen bonding between EG and maleic anhydride group of PP-*g*-MA [53]. Moreover, the incorporation of EG into maleated PP shifts the T_g to higher temperature. The increased in T_g is attributed to a decrease in mobility of the polymer chains, due to hydrogen bonding between the polar groups of PP-*g*-MA and EG.

Ramanathan et al. investigated the effects of different kinds of graphite particles on the thermomechanical behavior of PMMA–graphite nanocomposites [54]. The fillers used included “as received graphite” (denoted as ARG), mixed sulfuric/nitric acid treated EG and sonicated EG platelet (denoted as GNP). Figure 2.22 shows the variation of storage modulus with temperature for the PMMA–ARG, PMMA–EG, and PMMA–GNP nanocomposites reinforced with 1, 2, and 5 wt.% fillers. The glassy-state storage modulus (E') at 25 °C of PMMA–ARG nanocomposites at 1, 2, and 5 wt.% filler loading increases by 38, 100, and 110% over that of pure PMMA, respectively. The maximum increase in storage modulus vs. filler loading is obtained for the PMMA–GNP nanocomposites. At 5 wt.% GNP, the storage modulus is 133% higher than that of pure PMMA. Figure 2.23 shows the plots of $\tan \delta$ vs. temperature for pure PMMA, PMMA–ARG, PMMA–EG, and PMMA–GNP nanocomposites reinforced with 1, 2, and 5 wt.% fillers. The T_g increases are over 30 °C at 5 wt.% for ARG and GNP as a result of the interaction of graphite fillers with the PMMA matrix. It is noted that the maximum increase in T_g peaks appear at different loadings for different fillers: 1 wt.% for ARG, 2 wt.% for EG, and 5 wt.% for GNP. The decreasing T_g values with increasing filler content for the ARG- and EG-containing composites indicate that these fillers tend to agglomerate at higher loading.

For the epoxy–graphite nanocomposites, the storage modulus and glass transition also increase with increasing nanoplatelet loading [38]. Figure 2.24 shows the dynamic mechanical properties of pure epoxy and its nanocomposites [38]. At 30 °C, the 2.5 and 5 wt.% epoxy–graphite nanocomposites show about 8 and 18% higher storage modulus than the pure epoxy. The T_g s of pure epoxy, epoxy–2.5 wt.% graphite, and epoxy–5 wt.% graphite nanocomposites are 143, 145, and 146 °C, respectively. The increase in T_g is attributed to the good adhesion between the epoxy matrix and the nanoplatelets as the nanofillers restrict the segmental motion of cross-links under loading.

2.7 Electrical Behaviors

It is well recognized that the electrical conductivity of insulating polymers can be increased by the addition of conductive fillers such as carbon black and metallic particles. At low filler content, conducting fillers are dispersed within polymeric matrices as isolated clusters. In this case, the electrical conductivity of the composites is equal to or slightly higher than that of the polymer matrix. However, the electrical conductivity of polymer nanocomposites changes discontinuously with the filler content when their concentration reaches a critical value, known as percolation threshold (ϕ_c). As the loading level is increased above ϕ_c , a sharp increase of several orders of magnitude in the conductivity is observed. At this stage, the filler particles tend to connect each other to form continuous conduction paths within the composites, thereby allowing conduction of charge carriers. The transition from isolated cluster to connected network of conducting filler can be de-

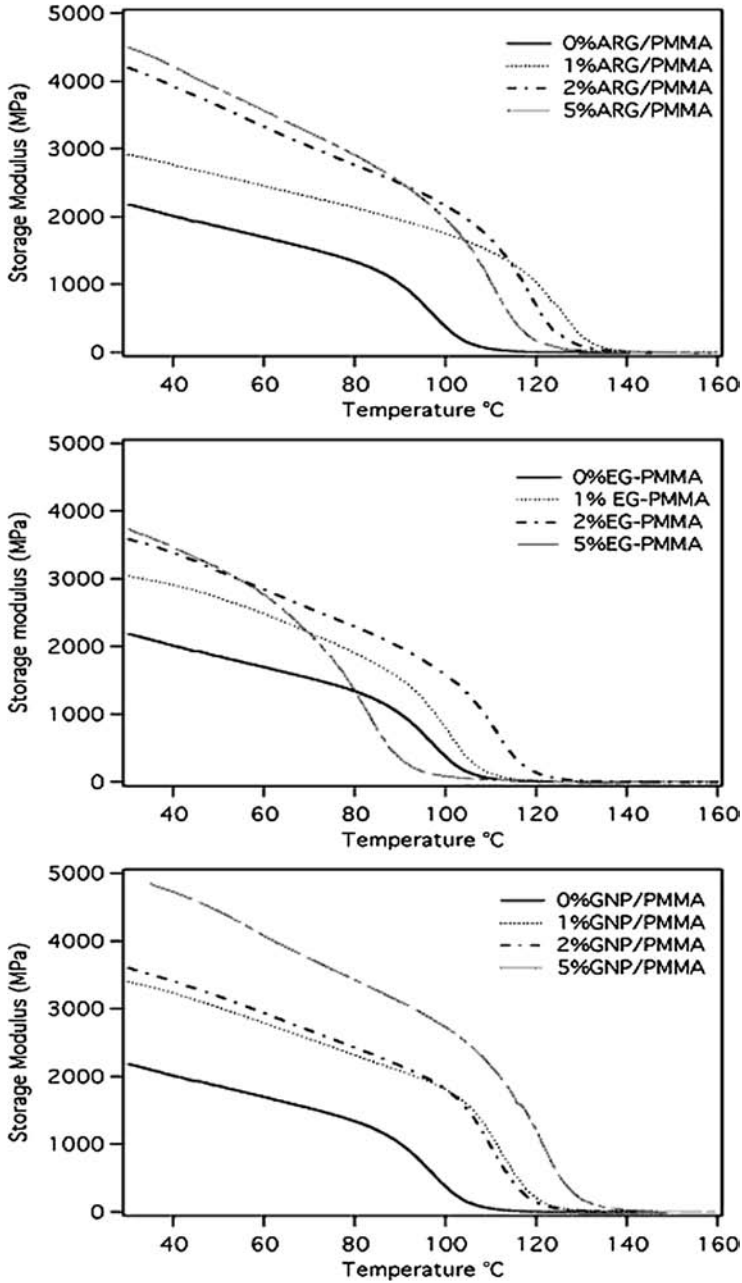


Figure 2.22. Plots of storage modulus vs. temperature for pure PMMA and the PMMA–graphite nanocomposites. Reprinted from [54] with permission of Wiley Interscience.

scribed by percolation theory [55,56]. Mathematically, the conductivity (σ) of composite materials can be described by a scaling law of the form

$$\sigma \sim (\phi - \phi_c)^t, \quad (2.4)$$

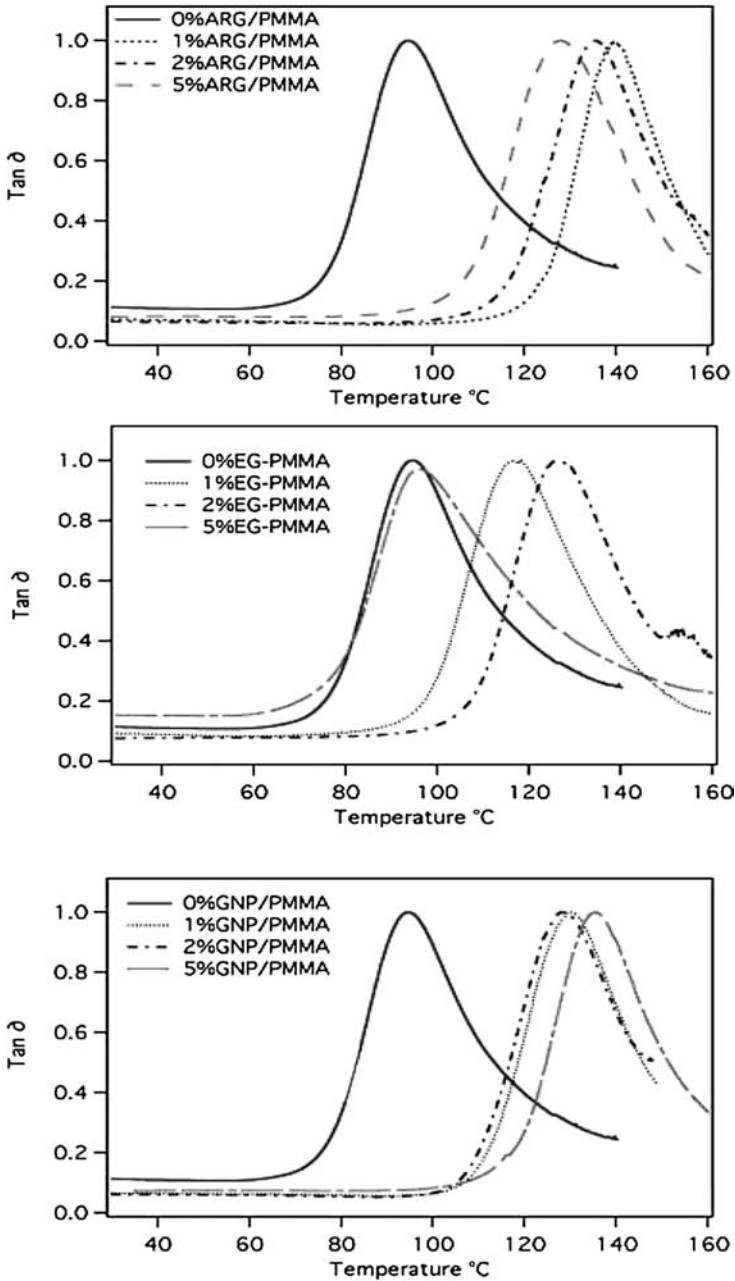


Figure 2.23. Plots of $\tan \delta$ vs. temperature for pure PMMA and the PMMA–graphite nanocomposites. Reprinted from [54] with permission of Wiley Interscience.

where t is the critical exponent. Equation (2.4) is valid when $\phi > \phi_c$ and $\phi - \phi_c$ is small.

Generally, large filler loading is needed to achieve percolation threshold in the polymer microcomposites. Nagata et al. studied the effects of graphite particle sizes on the electrical conductivity of low-density polyethylene (LDPE)–graphite microcomposites [57].

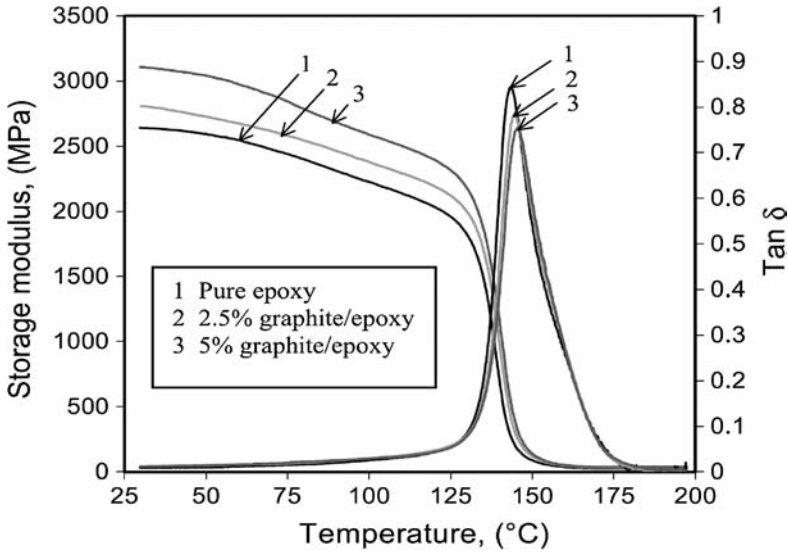


Figure 2.24. Plots of storage modulus vs. temperature and loss tangent vs. temperature for pure epoxy and its nanocomposites. Reprinted from [38] with permission of Elsevier.

The size of plate-like graphite ranged from 2.1 to 82.6 μm . They demonstrated that the percolation threshold concentration of filler in LDPE-graphite microcomposites is rather large. It varies from 13.5 to 25.5 vol.% depending on the size of graphite plates.

As demonstrated by Balberg, low-structure spherical particles require a much higher percolation threshold compared to high structure particles with large aspect ratios [58]. Therefore, very low filler percolation concentration is found for the polymer-graphite nanocomposites reinforced with EG of large aspect ratios [19,23,33,58,59]. Pan et al. [23] reported that the filler percolation threshold for the PA6-graphite nanocomposites prepared via intercalative polymerization is only 0.75 vol.%. More recently, Chen and co-workers have systematically studied the electrical behavior of PA6-graphite nanocomposites prepared via *in situ* polymerization [59–61]. They determined the percolation threshold of the PA6-graphite nanocomposites prepared via *in situ* polymerization of ϵ -caprolactam monomer and sonicated EG to be 0.74 vol.%. Figure 2.25 shows the plot of electrical conductivity vs. $\phi - \phi_c$ for the PA6-graphite nanocomposites. From this, the critical exponent can be determined, i.e., 2.32. The critical exponent of the PA6-graphite nanocomposites is larger than the most accepted universal value, i.e., $t = 2$ [55]. Chen et al. interpreted the higher value of critical exponent or nonuniversal behavior in terms of tunneling conduction [61]. Tunneling conduction is a thermal fluctuation assisted transport process. For the polymer-conducting filler composites, conduction can be described to thermal fluctuation induced tunneling of the charge carriers (i.e., electrons) through the insulating layer of polymer separating two neighboring fillers [62]. In this respect, the relation between the $\ln \sigma$ and $\phi^{-1/3}$ should be linear [63]. Figure 2.26 shows the variation of $\log \sigma$ with $\phi^{-1/3}$ for the PA6-graphite nanocomposites with EG content above the percolation threshold. It is apparent that the plot yields a straight line, indicating that tunneling conduction mechanism prevails in the PA6-graphite nanocomposites. This implies that tunneling takes place almost exclusively between very close, neighboring conductive nanosheets through a thin insulating polymer film. The conductivity of PA6 is rather low

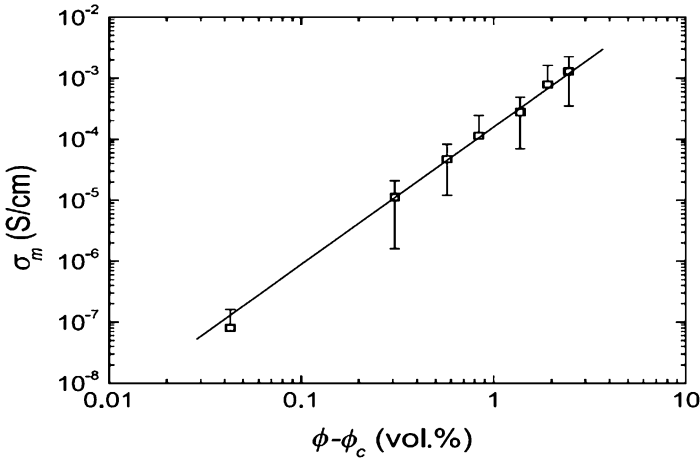


Figure 2.25. Electrical conductivities of the PA6–graphite nanocomposites as a function of $(\phi - \phi_c)$. Reprinted from [60] with permission of Elsevier.

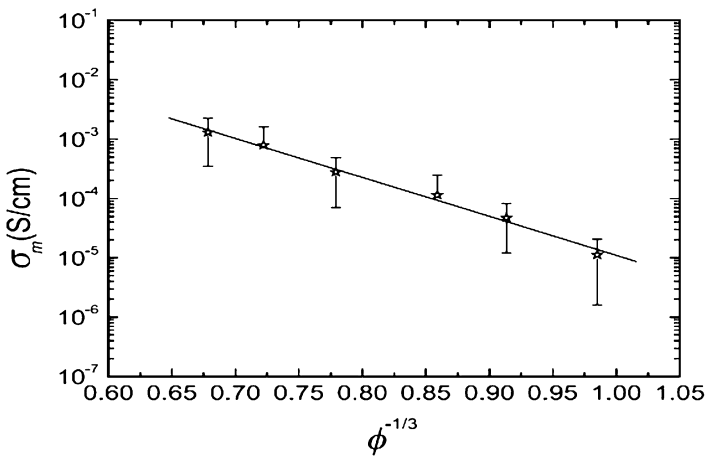


Figure 2.26. Variation of electrical conductivities with respect to $\phi^{-1/3}$ for PA6–graphite nanocomposites with filler content above the percolation threshold. Reprinted from [60] with permission of Elsevier.

having a value of 10^{-15} S/cm and approaches 10^{-3} S/cm for the nanocomposites with filler loading above percolation threshold.

It is noted that the processing techniques used to prepare the polymer–graphite nanocomposites can affect the filler percolation threshold. Shen et al. reported that the maleated PE–graphite nanocomposite prepared via intercalative polymerization exhibits lower percolation threshold than those fabricated by melt blending [34]. The dispersed graphite nanosheets of the solution intercalated nanocomposite possess a high aspect ratio. Consequently, conductive filler networks can be formed more easily in a polymer matrix at low percolation threshold. However, the graphite nanosheets of maleated PE–graphite nanocomposites prepared via melt intercalation exhibit nonuniform thickness and lower aspect ratio as mentioned previously.

2.8 Thermal Properties

It is well recognized that the physical and mechanical performances of semicrystalline polymer nanocomposites depend on the morphology, the crystalline structure, and degree of crystallization of polymers. The incorporation of nanofillers into semicrystalline thermoplastics would affect their melting and crystallization behavior. Chen and co-workers studied the crystallization kinetics and melting behaviors of PA6–1.5 wt.% graphite nanocomposite [24]. They reported that the foliated graphite nanosheets increase the crystallization temperature and half-time of crystallization of PA6. The nanosheets are considered to be acting as nucleating agents for PA6 crystals. Moreover, DSC melting traces show that the equilibrium melting temperature of pure nylon 6 is higher than that of the nanocomposite sample. They explained this in terms of the foliated graphite nanosheets hinder the motion of PA6 molecular chains, thereby forming less perfection of the crystals in the nanocomposite. More recently, Causin et al. reported that a structural change from α - to γ -phase occurs in PP due to a reduction in the molecular chain mobility by graphite nanoparticles [64].

In recent years, the demand for lightweight polymer composite materials with high thermal conductivity and low coefficient of thermal expansion (CTE) for applications in circuit boards, heat sinks in electronic packaging, appliances, and machinery is increasing in industrial sectors. Carbonaceous materials such as graphite platelets and carbon nanotubes generally exhibit excellent thermal conductivity. They are ideal filler materials for polymers having low thermal and electrical conductivity. Furthermore, graphite flakes have higher thermal diffusivity than polymers and their additions certainly improve thermal diffusivity of composites [65]. Hung et al. indicated that graphite nanoplatelets are beneficial in improving the thermal conductivity of an epoxy resin (Epon 862) [66]. The effectiveness of EG in enhancing the thermal conductivity of Epon 862 resin has also reported by Debelak and Lafdi very recently [67]. Debelak and Lafdi demonstrated that the CTE values of the graphite–epoxy nanocomposites tend to decrease with increasing graphite content. Exfoliated graphite has a lower CTE value than the epoxy, thus mixing them together can create a polymer nanocomposite with lower CTE values. Figure 2.27 shows the variation of thermal conductivity with EG content for the graphite–epoxy nanocomposites. Exfoliated graphite platelets of different sizes are used. The large graphite flake polymers have a threshold at 3 wt.%, while medium and small have thresholds at 6 and 10 wt.%, respectively. The larger graphite nanoplatelets have larger aspect ratios, enabling the formation of a conducting network more easily. At 20 wt.% graphite, the three exfoliated graphite filled epoxy nanocomposites exhibit a very close thermal conductivity value of about $4.3 \text{ W m}^{-1} \text{ K}^{-1}$. This value is nearly 2000% increase over the pure epoxy ($0.219 \text{ W m}^{-1} \text{ K}^{-1}$).

The incorporation of small amounts of inorganic fillers into polymers generally improves their thermal stability and flammability properties. Typical example is the clay silicate additions that lead to higher heat distortion temperature (HDT) of PP [68]. Polymer–clay nanocomposites are known to display excellent flame retardant characteristics [69]. In the case of polymer–graphite nanocomposites, low loading levels of graphite platelet generally increase the 5 and 10% weight loss temperatures ($T_{-5\%}$; $T_{-10\%}$) of the materials on the basis of thermogravimetric analysis [25,35,38,48].

The issue of flammability of polymers is becoming a matter of great concern. EG is considered an attractive material that can provide good fire retardancy to many polymers. The burning behavior of polymers is expressed in terms of their ability to generate flammable volatile products subject to thermal combustion. The burning process of a polymer

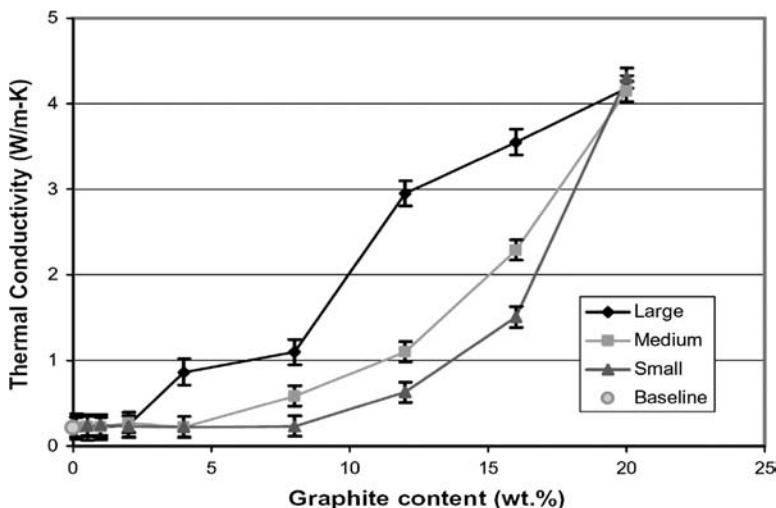


Figure 2.27. Thermal conductivity of exfoliated graphite filled epoxy with different graphite flake sizes as a function of graphite content. Reprinted from [67] with permission of Elsevier.

generally begins with heating to a temperature at which thermal degradation initiates. The cone calorimeter is the most effective methods for studying the flammability of materials. The peak heat release rate (PHRR) obtained from the cone calorimetric measurement is often used to evaluate the maximum amount of energy that a material may release during combustion. According to the literature, the PHRR values of polymers are decreased considerably by adding the graphite platelets [35,48,70–72]. The reduction in the PHRR is attributed to the formation of a high performance char barrier layer that retards mass transfer of degrading polymer to the vapor phase. The barrier also shields the underlying polymer from the external thermal radiation, acting as a thermal insulation layer.

2.9 Conclusion

Graphite is a layered solid consists of aggregate of graphene layers in which the carbon atoms are covalently bonded in hexagonal arrays. Graphite nanoplatelets can be synthesized by a relatively simple intercalation and exfoliation process. They can be produced either from the electron-donor agents such as alkali metals, or from the electron-acceptors such as oxidizing agents. Potassium intercalant has been used to form a first stage intercalation compound KC_8 . The KC_8 compound can be further exfoliated in ethanol to produce graphite nanoplatelets of 40 layers thick. Alternatively, graphite oxide intercalation compound can be prepared via oxidation of graphite in sulfuric acid in the presence of an oxidizing nitric acid. The GO is then rapidly heated by means of either resistive/induction furnace, infrared, microwave, or laser irradiation to form the expanded graphite. The exfoliated nanoplatelets with large surface area and aspect ratio, high electrical and thermal conductivities are ideal fillers for polymers to produce-conducting nanocomposites. Such novel composite materials only require a very low EG content to achieve high electrical conductivity. For example, the percolation threshold of PA6–graphite nanocomposites prepared via *in situ* polymerization is only 0.74 vol.%. Incorporating expanded graphite into PP markedly improves its flexural strength and stiffness as well as impact strength. How-